the plant journal

Dissecting the molecular mechanism of russeting in sand pear (Pyrus pyrifolia Nakai.) by metabolomics, transcriptomics and proteomics

Journal:	*The Plant Journal*
Manuscript ID	TPJ-00957-2021.R1
Manuscript Type:	Original Article
Biochemistry and Physiology:	Fatty acid metabolism < Lipid metabolism
Cell Biology:	Epidermis / cuticle
Genomics & Genetics:	None of the below
Plant Growth & Development:	None of the below
Plant interactions with other organisms:	None of the below
Plant Responses to Environment:	Metabolic adaptation to stress < Abiotic stress
Other (please specify):	

SCHOLARONE™
Manuscripts

Dissecting the molecular mechanism of russeting in sand pear (*Pyrus pyrifolia* Nakai.) by metabolomics, transcriptomics and proteomics

Chun-hui Shi[1,2], Xiao-qing Wang[1], Jian-feng Xu[2], Yu-xing Zhang[2*], Baoxiu Qi[2,3,4*], Jun Luo[1*]

[1] Forest & Fruit Tree Research Institute, Shanghai Academy of Agriculture Sciences, Shanghai, 201403, China

[2]College of Horticulture, Hebei Agricultural University, Baoding, Hebei, 071001, China

[3]School of Pharmacy and Biomolecular Sciences, Liverpool John Moores University, James Parsons Building, Byrom Street, Liverpool L3 3AF, UK

[4]Beijing Advanced Innovation Centre for Tree Breeding by Molecular Design, Beijing University of Agriculture, 7 Beinong Rd, Changping District, Beijing, China

CONFIDENTIAL

Correspondence authors:

Yu-xing Zhang, Email: zhangyuxing7199@163.com

Baoxiu Qi, Email: b.qi@ljmu.ac.uk

Jun Luo, Email: zuowusuo@163.com

SUMMARY

The brown colouration and rough appearance as russet and semi-russet (partial russet) are features unique to the popular Asian sand pear (*Pyrus pyrifolia* Nakai.). The degree of russeting is different between different genotypes. Russeting is sensitive to water fluctuations, where excessive rainwater can trigger/elevate its development. However, the molecular mechanism of russeting is currently unclear. Here, we employed multi-omics, i.e., metabolomics, transcriptomics and proteomics and analyzed the effect of different sand pear genotypes and artificial rainfall on russeting of pear fruits. This led to the identification of 79, 64 and 29 differentially produced/expressed metabolites, transcripts and proteins that are involved in the biosynthesis of suberin, phenylpropane, cutin and waxes. Further analysis of these differentially expressed genes and their encoded proteins revealed that four of them exhibited high expression at both transcript and protein levels. Transient expression of one such gene, *PbHHT1* (accession number 103966555) that encodes for ω-hydroxypalmitate-O-feruloyl transferase (HHT) in the young green non-russet fruits triggered premature suberization in the russeting pear genotypes. This coincided with the increased production of 16-feruloyloxypalmitic acid, a conjugated compound between phenols and esters during the polymerization for suberin formation. Collectively, our data from the combined three omics demonstrates that russeting in sand pear is a complex process involving the biosynthesis and transport of suberin and many other secondary metabolites.

Keywords: sand pear, russeting, multi-omics, suberin, rainfall, *PbHHT1*

CONFIDENTIAL

INTRODUCTION

Fruit colour, a key indicator for quality, is a major factor affecting consumer choice (Gamble *et al.*, 2006). Russet and semi-russet (partial russet) color is unique to sand pear (*Pyrus pyrifolia* Nakai.) which is native to Eastern Asia, including China, Japan and Korea. However, in recent years it has also gained popularity in other countries, such as India, Australia, New Zealand and the United States.

Similar to many other fruits such as apple, the peel colour of pears are usually determined by anthocyanins. However, the brown colour exhibited on the peel of sand pear fruits is thought to be due to the accumulation of suberin lamellae (SL) caused by the defective cuticle developed on the otherwise green peel (Inoue *et al.*, 2006, Wang *et al.*, 2014a). Suberin, the main component of SL is a cutin analog and is primarily composed of C_{16}-C_{26} long chain fatty acids (LCFAs) and phenolics linked with alkyl ferulate-waxes. It is polymerized from a range of compounds, such as glycerol, fatty acids (FAs), phenols, suberin-related waxes, lignin, tannins and other phenolics (Franke and Schreiber, 2007, Pollard *et al.*, 2008). Both suberin lamellae and stratum corneum (SC) have similar functions in protecting the fruit from damage. However, SL is more plastic under environmental stress (Riederer and Schreiber, 2001, Lara *et al.*, 2015). For example, in rice (*Oryza sativa* L.), the deposition of SL in the root was induced by salt-stress where its accumulation was negatively correlated with the transportation of salt to the shoot from the root (Krishnamurthy *et al.*, 2011). In Arabidopsis the synthesis of suberin is mediated by stress hormones such as abscisic acid and ethylene in the root, indicating a positive role of stress on russeting (Barberon *et al.*, 2016). Studies also showed that lignin, cellulose and hemicellulose were significantly higher while pectin polysaccharides and long-chain fatty acids were lower in russet compared to green non-russet pears, indicating that these compounds also play roles in pear russeting (Heng *et al.*, 2014, Wang *et al.*, 2014a).

CONFIDENTIAL

Many candidate genes involved in suberin biosynthesis in both russet pears and apples have been identified via transcriptional analysis, including genes encoding for BAHD family acyltransferase, ω-hydroxypalmitate-O-feruloyl transferase (HHT), glycerol phosphate acyltransferase (GPAT), 3-ketoacyl-CoA synthase (KCS), ATP binding cassette (ABC) transporters, MYB93-like transcription factors and acyltransferases. Genes involved in lignin biosynthesis such as those encoding for Caffeic acid 3-O-methyltransferase (COMT), Caffeoyl CoA-O-methyltransferase (CCOAOMT), Cinnamoyl-CoA reductase (CCR), Cinnamyl alcohol dehydrogenase (CAD) and Peroxidase (POD) were also found in transcriptome datasets in both russet apple and pear fruits (Justin *et al.*, 2015, Legay *et al.*, 2015, Wang *et al.*, 2016, Hou *et al.*, 2018).

Studies by combined high-throughput omics, such as genomics, transcriptomics, proteomics, and most recently, metabolomics, have been employed to study complex signaling pathways including russeting in many plants in recent years (Cohen *et al.*, 2017, Jia *et al.*, 2019). For example, the cuticular membrane and the periderm membrane between the russet pear 'Niitaka' and its green non-russet mutant 'Suisho' were compared at both transcript and protein levels in order to dissect the russeting mechanisms. It was found that both the transcript and protein levels of *GLP* (Germin-like protein) gene were higher in the russet 'Niitaka' than the green 'Suisho' fruits, indicating that GLP, which is related to jasmonic acid (JA) signaling pathway could promote periderm membrane synthesis hence russeting in 'Niitaka' pear fruits (Wang *et al.*, 2020).

Previously, we showed that russeting in sand pear fruit was triggered and enhanced by suberin lamellae accumulation upon excess water application, mimicking heavy rainfall. A sharp increase in lignin content in the russet fruit peel was detected, which was coincided with the increased expression levels of proteins related to the biosynthesis of phenylalanine, the lignin monomer, as well as those related to defense (Shi *et al.*, 2019). In order to further understand the molecular regulatory network of russeting in sand pear fruit we took

SUBMITTED MANUSCRIPT

CONFIDENTIAL

advantage of the recently developed multi-omics techniques to compare the differences in russeting between: (1) three different genotypes, i.e., the russet 'Zaoshengxinshui' pear (ZS), the semi-russet 'Cuiguan' pear (CG), and the green non-russet 'Cuiyu' pear (CY); (2) rainfall- and non-rainfall treatment on the russet ZS and semi-russet CG fruits. By combining the three datasets of metabolomics, transcriptomics and proteomics we created a comprehensive molecular network showing changes in major metabolites, genes and proteins related to russeting in sand pear fruit. Importantly, a number of putative genes and their encoded proteins involving in russeting were identified where one of them, *PbHHT1* was experimentally confirmed to be involved in russeting in sand pear fruit. This is expected to provide a rich resource for future in-depth study into the mechanism of russeting in pear and perhaps other fruit, such as apple.

CONFIDENTIAL

RESULTS

Phenotypic analysis of russeting in the sand pear fruits

Russeting is a unique feature of sand pear fruit which is believed to be mainly due to the accumulation of suberin lamellae its peel. Different degrees of russeting are found between different colored sand pear genotypes. Indeed, our observations show that on maturity the peel of the russet ZS fruit was fully covered by brown spots with a russet index of 100% (full russet), the semi-russet CG fruit were also largely covered and the russet index was 85% while no russet was present on the green non-russet CY fruit where the russet index was close to 0% (Fig. 1A&1D). It is noteworthy that there was still a localized green background remaining on the peel of both ZS and CG fruit despite their high russet indexes.

Scanning electron microcopy (SEM) observation of the ZS fruit peel revealed that the stratum corneum (SC) was cracked into small pieces, and these cracks extended to reach the epidermal cells. The cuticle cracks were also evident in the peel of the semi-russet CG fruit where they were filled with cork tissues. However, in the peel of the green non-russet CY fruit where no russet spots were formed, the cuticle was smooth with no obvious cracks shown (Fig. 1A, middle panel). Ultra-thin sections were prepared from the plastic embedded peels of these three genotypes of fruit and observed by transmission electron microscopy (TEM). This showed that the epidermal cells of the russet and semi-russet fruit peel were filled with flocculent tannin cells (TC). However, those of the green non-russet pear fruit were rich in liposomes (LAMB), which were surrounded by small lipid droplets which were scarce in the russet and semi-russet pear fruit (Fig. 1A, right panel).

The phenotype of the rainfall-treated fruit was also investigated. It was found that rainfall treatment aggravated russeting in the ZS and CG fruit (Fig. 1B). The SL in the peel of the semi-russet CG was enlarged and that of the russet ZS became even thicker compared to the non-rainfall-treated controls (Fig. 1E and 1F;

CONFIDENTIAL

Fig. S1). The russet index of the rainfall treated semi-russet CG fruit reached 93% compared to 30% in the non-treated control fruit, i.e., three times higher than the controls. The thickness of SL was 87 µm in the rainfall-treated russet ZS fruit, double that of the non-rainfall-treated fruit (43 µm) (Figs. 1E and 1F; Fig. S1). Extensive cracks were also apparent on the epidermal cuticle of the ZS fruit peel where the most severe cracks led to shedding, epidermal damage and SL formation. Although there were also cracks formed in the epidermal cuticle of the non-treated control fruit they were not filled by the suberized cells as observed in the rainfall-treated fruit (Fig. 1C).

Analysis of differentially expressed metabolites (DEMs) in sand pear fruit

In order to identify the macromolecules related to sand pear fruit russeting we first performed UPLC-Q-TOF/MS (Ultra-performance liquid chromatography/time-of-flight mass spectrometry) metabolomic analysis and found a total of 3,391 metabolites from the mature pear fruit peel. Principal Components Analysis (PCA) revealed clear differences between the three pear genotypes as well as between rainfall-treated and non-rainfall-treated controls from the same russet and semi-russet fruit (Fig. S2). After combining the results of Partial Least Squares Discriminant Analysis (PLS-DA) modeling and the student's *t*-test (Perez-Enciso *et al.*, 2003), 611 and 430 DEMs were identified between the peel of the russet ZS and the semi russet CG, and the green non-russet CY fruit, respectively. Three hundred and sixty-three (363) DEMs were identified between the rainfall treated ZS and 320 in CG pear fruit and the non-treated controls (Fig. 2B). Subsequent KEGG (Kyoto Encyclopedia of Genes and Genomes) enrichment analysis showed that these DEMs were the main components for the biosynthesis of secondary metabolites, such as cutin, suberin, wax, long chain fatty acids and phenylpropanoid (Fig. 3A). Importantly, 70 DEMs were found to be common between all the russet samples (Fig. 2A and table. S1).

CONFIDENTIAL

Further analysis clustered these DEMs into 7 functional groups, i.e., phenolics, fatty acids, lipids, terpenoids, ester, fatty alcohol and glycerol (Fig. 2A and table S1). Higher levels of phenolics were found in the russet ZS and semi-russet CG and their rainfall-treated fruit compared to the green non-russet CY and the non-rainfall-treated controls (Fig.2A, 2C and table S1). The lignin, (±)-catechin, epicatechin and ferulic acid were all significantly higher in the russet and semi-russet, as well as in the rainfall-treated fruit compared to the non-russet and no-rainfall-treated fruit (Fig. 2A, 2C and Fig. S3). A similar trend was found with the ω-6 polyunsaturated long chain fatty acids, such as 3E, 9Z, 12Z-octadecatrienoic acid and 5Z, 9Z, 12Z-octadecatrienoic acid, the ω-9 unsaturated fatty acids oleic acid (9Z-octadecadienoic acid) (C18:1n-9), α,ω-diacids (eicosadienoic acid), and the ω-OH fatty acids, hydroxy fatty acids (24-hydroxy-tetracosanoic acid) (Fig. 2C and Fig. S3). The levels of palmitic acid (C16:0) and its acylglycerides (2-palmitoylglycerol) were also higher in the rainfall-treated russet ZS and semi-russet CG than those in the non-treated control fruit (Fig. S3). On the contrary, very long chain alkanes such as triacontane were decreased remarkably ($p < 0.05$) in the peel of russet ZS and semi-russet CG, as well as in their rainfall-treated than the non-russet CY and non-rainfall-treated fruit (Fig. 2C).

CONFIDENTIAL

Transcriptome profiling of the peels of sand pear fruit

To see changes in transcript levels of genes related to russeting, transcriptome analysis was performed using the same samples as for the metabolome analysis described above. After quality assessment and data filtering, a total of 7,630 transcripts were found differentially expressed between russet ZS and non-russet CY fruit (ZS vs CY), 5,171 between the semi russet CG and non-russet CY (CG vs CY), 803 between the rainfall-treated and non-treated control russet ZS (ZS-R vs ZS-C), and 1,718 between the rainfall-treated and non-treated semi-russet (CG-R vs CG-C) fruit. Using KEGG pathway analysis we found that the differentially expressed

genes (DEGs) that were common between the two russet genotypes as well as between the rainfall-treated samples were those involved in the four main biosynthesis pathways involved in (1) secondary metabolites; (2) cutin, suberin and waxes; (3) very long-chain fatty acids, and (4) phenylpropanoid. In addition, genes encoding for ABC transporters were also found among the common DEGs (Fig. S2).

We next carried out a comparative analysis of all the data generated from samples of the three genotypes as well as those from the rainfall-treated and non-rainfall-treated control fruit. This led to the identification of 64 common DEGs where 13 were related to the biosynthesis of cutin, suberin and waxes (Fig. S5 and Table S2). Further comparison and verification of data consistency resulted in the discovery of a few important genes that showed significant changes in their transcript levels (Table 1). Notably, the transcript level of *PbHHT1* (acc no. 103966555) was 2.7- and 3.7-fold higher in the russet ZS and the semi-russet CG compared to the green non-russet CY fruit, respectively (Table 1 and Fig. 4C). Rainfall treatment also enhanced the expression level of this gene where its transcript level increased by 0.2-fold in the russet ZS and 3.2-fold in the semi-russet CG fruit respectively, compared to the untreated controls. A second gene, *PbCYP749a22* (acc no. 103948102), one of the important regulatory genes of cytochrome P450 monooxygenase, was also significantly higher in the russet ZS (5.1-fold) and semi-russet CG (3.5-fold) compared to the green non-russet CY fruit. However, rainfall treatment increased transcript levels in the russet ZS (ZS-R) (1.1-fold), but not in the semi-russet CG fruit. Beta-keto ester CoA synthetase (KCS) is an integral part of the fatty acid elongase complex (FAE). It was found that *PbKCS10-like* (acc no. 103949661) showed markedly lower expression in the peel of the russet ZS and semi-russet CG fruit, as well as in its rainfall-treated fruit. Similarly, *PbCER1-like* (acc no. 103929753) and *PbWSD1-like* (acc no. 103928845) that possibly have roles in the biosynthesis of wax esters, were also significantly downregulated in the peel of both russet ZS and semi-russet CG and their rainfall-treated fruit.

CONFIDENTIAL

Different expression profiles of many genes involved in the biosynthesis of lignin were found between the fruit of the two russet and the green non-russet genotypes. For example, the transcript level of *PbCAD1* (acc no. 103951782) was higher in the peel of both the russet ZS and semi-russet pear CG than the non-russet CY fruit. The expression levels of *PbCOMT1* (acc no. 103927980) and *PbCCoAOMT* (acc no. 103933993) were significantly higher in the peel of the russet ZS fruit, while that of *PbCOMT2* (acc no. 103951572) was significantly higher in the peel of the semi-russet CG fruit compared to the non-russet CY fruit. Suppressing the activity of CCR could lead to lignin-monomer loosening and promote the movement of phenolics, such as ferulic and sinapic acids to the cell wall (CW), causing russeting in pear (Wang et al., 2014a). In line with this we also found that the transcript level of *PbCCRSNL-like* (acc no. 103943280) was lower in the peel of the russet and semi-russet, also in their rainfall-treated fruit compared to the controls.

ABC transporters and lipid transfer proteins (LTPs) are the primary proteins that are involved in the transmembrane transport of cutin and wax to the cell wall. Notably, genes encoding for the G family members of the ABC transporters exhibited lower- (*PbABCG15*, acc no. 103942099), or higher- (*PbABCG10*, acc no. 103934278) expression levels in the russet ZS and semi-russet CG than in the green non-russet CY fruit. Treatment by rainfall resulted in similar trends in their expression profiles (Table S2). Further, the transcripts of both *PbnsLTP* (acc no. 103938613, 103961206) and *PbnsLTP-like* (acc no. 103961207) showed significantly lower levels in the russet and rainfall-treated than their controls, indicating that the transmembrane transport of cutin and wax to CW were less efficient in the russet and rainfall-treated fruit than the control (Fig. 4B and 4C). This may lead to the accumulation of these compounds, resulting in russeting in the russet and rainfall induced russet ZS and semi russet CG fruit.

Altered transcript levels of genes involved in fatty acid biosynthesis were also detected in the rainfall-treated russet and semi-russet fruit. For example, the transcript levels of both *PbGPAT5* (glycerol-3-phoshate acyltransferase 5, acc no. 103942961) and *PbFAR3* (fatty acyl-CoA reductase, acc no. 103931004) were

CONFIDENTIAL

significantly higher than in the control fruit (C groups). *PbKCS19* (acc no. 108865656), *PbKCS10* (acc no. 103952998) and *PbKCS20* (acc no. 103940571), which all participate in fatty acid elongation, were all lower in the rainfall treated fruit of the russet fruits compared to the untreated fruit. Genes encoding for cytochrome P450 monooxygenase, oxidoreductase (*PbP45086A8*, acc no. 103957382) and fatty acid elongase (FAE) (*PbP45086B1*, acc no. 103943216) in the semi-russet CG fruit were significantly upregulated compare to those of the controls (Fig. 4C). Therefore, it seems that altered fatty acid biosynthesis is involved in the rainfall induced russeting in sand pear fruit.

Expansins and aquaporins are both non-enzymatic proteins that are believed to play roles in water stress by changing the CW structure and the water channels of the cell membrane (Li *et al.*, 2015, Secchi *et al.*, 2017). In line with this, genes encoding for expansin, a protein that relaxes plant cell walls, including *PbExpA*$_4$ (acc no. 103954300) and *PbExpB15* (acc no. 103959804), showed higher expression levels in the peel of the russet ZS and semi-russet GS fruit under rainfall-treatment (Fig. 4C). The transcript levels of the three aquaporin genes, *PbTIP1-3* (acc no. 103930703), *PbPIP2-2* (acc no. 103956770) and *PbPIP2-5* (acc no. 103937541), as well as the Dehydrin 3 encoding gene *PbDHN3* (acc no.103937812) were all upregulated in the peel of russet and semi-russet pears. Therefore, it appears that rainfall can cause cell wall relaxation by enhancing the expression of these genes.

Proteome profiling of the peels of sand pear fruits

We also profiled and analyzed the differentially expressed proteins (DEPs) by iTRAQ from the same samples as described for the RNA-seq above. Two hundred and sixty-eight (268) DEPs were identified between the russet ZS and non-russet CY (ZS vs CY) and 241 DEPs between the semi russet CG and non-russet CY (CG vs CY). In the rainfall treated fruit, 121 and 85 DEPs were identified between the treated ZS and CG fruit and the non-treated controls, respectively. Further comparison and analysis of these DEPs led to the discovery of

CONFIDENTIAL

23 DEPs that could be related to russeting of sand pear fruit (Table S3). They were again compared against the common DEGs identified from the RNA-seq analysis from above. This resulted in the discovery of 4 candidates that were differentially expressed at both the protein and transcript levels: PbHHT1/*PbHHT1*, PbKCS10 /*PbKCS10*, PbnsLTP3/*PbnsLTP3* and PbnsLTP4/*PbnsLTP4*. Interestingly, these four DEPS are related to the biosynthesis of cutin, suberin and wax as well as to stress (Table 2). The relative expression levels of these four co-expressed DEPs and DEGs were analyzed by targeted proteomics by PRM (Parallel Reaction Monitoring) and showed that those of PbHHT1, PbnsLTP3 and PbnsLTP4 were consistent with their absolute expression levels where the expression of PbHHT1 was enhanced, while PbnsLTP3 and PbnsLTP4 were significantly depressed in the peel of rainfall-treated russet and semi-russet pear fruit compared to the non-treated controls (Fig. 5).

CONFIDENTIAL

PbHHT1 plays essential roles in russeting in sand pear fruit

Because both the expression levels of the transcript and protein of *PbHHT1* were significantly higher in the russet and semi-russet, as well as in the rainfall-treated compared to the non-russet and non-treated fruit, we next carried out experiments to verify the function of *PbHHT1* in pear russeting. This was done by transiently expressing *PbHHT1* in the young non russet green fruit of the semi-russet CG and the non-russet CY by injecting the 35S:*PbHHT1* containing transgenic Agrobacterial solution. Controls of the empty vector containing Agrobacteria (EV), infiltration buffer (MMA) and water were included for comparison.

As shown in Figure 6A, after injection of 35S:PbHHT1 containing transgenic agrobacteria russeting of the peel (SL accumulation) and lenticel suberization were clearly observed on the peel of the young semi russet CG fruit. The lenticel suberinization was also intensified and the filamentous-like russet around the

injection site was observed in the CY peel. However, no SL accumulation and/or lenticel subrinization were present in the peel of other controls (Fig 6A, top panels). To visualize the presence of suberin in the peel, they were stained with berberine-aniline blue and observed under a fluorescence microscope. A large area of strong blue fluorescent signal was observed showing the suberin layer in the peel of CG fruits that was injected with the *PbHHT1* containing agrobacteria. However, in the peel of the control fruit only a weak and scattered blue light staining was observed showing the lenticels (Fig 6A, bottom panel, arrows).

In order to determine whether the observed accumulation of suberin was indeed due to the overexpression of *PbHHT1* in the peel of injected fruit, we carried out qRT-PCR on RNAs isolated from the tissue covering the injection sites (arrows in Fig 6A, top panel). The results showed that the transcript levels of *PbHHT1* was up-regulated by 6.7- and 2.5-fold in the CG and CY fruit respectively, injected with the *PbHHT1* containing transgenic agrobacteria, while no such changes were observed in the control fruit injected with the EV, MMA and water (Figure 6B).

Next, we analyzed the metabolites in the transgenic peel expressing *PbHHT1* and found that the content of the suberin monomer was increased significantly in both the CG and CY fruit peel. However, the amount of ω-feruloyloxypalmitic acid was 2.63 times higher in the *PbHHT1* expressing CG peel than in the CY peel (2.16μg/g in CG compared to 0.57μg/g in CY fruit) (Fig. 6B). Therefore, the combined results above clearly demonstrated that russeting in sand pear fruit was closely related to the high expression levels of *PbHHT1*. This led to the increased production of ω-feruloyloxypalmitic acid, the suberin monomer hence russeting in the fruit.

To understand the effect of *PbHHT1* on triggering russeting in young green fruit, RNA-seq was carried out to monitor the altered expression profiles of relevant genes. It was found that in addition to the significantly up-regulated transcript level of *PbHHT1* in both CG and CY fruit, the *PbCYP86A8* (acc no.103957382), a

CONFIDENTIAL

gene upstream of *PbHHT1* in the suberin biosynthesis pathway and *PbGPAT5* were also significantly up-regulated in the *PbHHT1* overexpressing CG and CY fruit peel. However, the expression of some russeting related genes was only significantly changed in the CG but not in the CY fruit peel (Figure. 6D). For example, lignin synthesis related gene *PbCOMT1* was upregulated, while *PbCCRSNL-6* was downregulated in the CG but not the CY fruit. Genes related to fatty acid elongation and wax biosynthesis, such as *PbKCS19*, *PbKCS10*, *PbKCS20*, *PbCER1-like*, *PbWSD1-like*, *PbnsLTP* and *PbnsLTP-like* were all down-regulated in the semi-russet CG whilst they showed no significant changes in the non-russet CY fruit. Genes encoding for expansins such as *PbExpA4* and *PbPIP2-2* were upregulated in the peel of the semi-russet CG but not the CY fruit.

Therefore, it seems that the gene expression profiles in the premature russetting of CG fruit peel caused by transient expression of *PbHHT1* were very similar to those observed in the rainfall triggered russetting in the sand pear fruit, as described earlier.

CONFIDENTIAL

Comparative analysis of all the data generated from metabolome, proteome and transcriptome

Because russeting occurred in the russet ZS and semi-russet CG fruit and this was enhanced/triggered by rainfall, we integrated all the data obtained from the metabolome, transcriptome and proteome by converting and mapping the genes, proteins and metabolites into the KEGG database. This resulted in the identification of 103 DEGs, 18 DEPs and 8 DEMs that are common between all the russet and non-russet control samples. Further analysis indicated that they are all involved in the biosynthetic pathways of secondary metabolites (Fig. 7). These DEGs, DEPs and DEMs were further grouped into 5 clusters (I–V) according to the specific metabolites that they are associated with. Cluster I includes genes and proteins mainly involved in the biosynthesis of phenylpropanoid (CAD1, PER53, COMT1, BGLU17), cluster II for cutin, suberine and wax

(HHT1, KCS4, CER1), cluster III for fatty acids (ADH2, FAD2), cluster IV for flavonoid (LDOX, CHS) and cluster V for fatty acid elongation (CUT1, KCS4, KCS2, KCS12) (Table S5 and S6). Interestingly, higher expression levels of DEGs, DEPs and DEMs in clusters I–IV (such as CAD1, BGLU17, HHT1, and COMT1) while lower expression levels of those in cluster V (such as CUT1, KCS4) were detected in the russet and semi-russet, as well as in their rainfall-treated fruit compared to their relevant controls (Fig. 7).

Taken together, our data from the combined 3 omics demonstrate that russeting in sand pear fruit is regulated by the biosynthesis of phenylpropanoid, suberin, wax, fatty acids, flavonoid and their polymerization components. Furthermore, heavy rainfall can aggravate russeting by up- or down-regulating the expression of relevant genes and proteins, resulting in the accumulation and polymerization of these secondary metabolites.

CONFIDENTIAL

DISCUSSION

The russet colour is a special feature of sand pear fruit and is thought to be due to suberin lamellae coverage on the fruit peel. Indeed, we demonstrated here that in the russet fruit of sand pear, the cracks of the stratum corneum on the peel were filled by the suberized cells while this was not observed in the green non-russet fruit (Fig 1). As the major structural compound of SL suberin is a complex heteropolymer formed from aromatic substances including phenols, hydroxycinnamic acids, ferulic acid, cinnamic acid and lignin, it also contains a large amount of aliphatic polymers produced from ω-hydroxy fatty acids. These aliphatic compounds have been previously identified in pears and apples (Franke and Schreiber, 2007, Pollard *et al.*, 2008, Legay *et al.*, 2015, Vishwanath *et al.*, 2015). Suberin lamellae not only affects the coloration of the pear fruit but it is also evolved to protect plants from damage caused by harsh environment, such as heavy rainfall (Lara *et al.*, 2015, Shi *et al.*, 2019).

In this study, we first carried out metabolome profiling of sand pear fruit and found that phenols, lignin, ω-unsaturated fatty acids, α, ω-diacids, ω-OH fatty acids and glycerides were enriched in the peel of the russet pear fruit (Fig 3C and Fig S3). These compounds were confirmed to be the major components of suberin in Arabidopsis and potatoes (Franke and Schreiber, 2007, Li *et al.*, 2007, Serra *et al.*, 2014). The aliphatic compounds of suberin are mainly $C_{16–20}$ ω-hydroxy fatty acids (Bernards and Mark, 2002,Krishnamurthy *et al.*, 2011). Interestingly, while the components of suberin were variable between different species of *Quercus variabilis* Blume, *Picea fortunei* (*Pseudotsuga sinensis* Dode) and potato (*Solanum tuberosum* L.) the same C_{18} unsaturated fatty acids were always found in their suberin-rich tissues (Graça and Santos, 2010). Consistent with this we also detected high content of C_{18} unsaturated fatty acids in the russet peel of the artificial rainfall treated russet ZS and semi-russet CG pear fruit (Fig 3 and Table S1). Therefore, we propose that these C_{18} unsaturated fatty acids could be used as good indicators of the presence of suberin hence russet index in pear and perhaps other plant tissues/fruits in the future.

Consistent with the high level of C_{16-20} fatty acids (palmitic acid and dodecanoic acid) found in russet fruit peel, the expression levels of genes related to their biosynthesis, such as *PbGPAT5*, *PbCYP86A1* and *PbCYP86B1* were significantly upregulated (Figs 3&4A, Table S2). GPAT5 has specificity towards acyl-CoA substrates of C_{16-20} fatty acids and their ω-oxidized derivatives, the major determinants of suberin components (Yang *et al.*, 2012), while the CYP86 subfamily, including CYP86A4, CYP86A8, CYP86A1, and CYP77A6 catalyzes the ω-hydroxylation of C_{16} and C_{18} fatty acids in plants (Duan and Schuler, 2005; Wang *et al*., 2019). Therefore, the increase of oleic acid ($C_{18:1}$) and palmitic acid ($C_{16:0}$) in the suberin tissue we detected in the russeting sand pear fruit further confirms the role of CYP86 in suberin biosynthesis (Fig. S3). On the other hand, the very long chain alkane triacontane, C30 alkanes, the component of cutin and waxes in pear fruit (Norris and Bukovac, 2010, Wang *et al.*, 2014b) was extremely reduced in the rainfall-

SUBMITTED MANUSCRIPT

CONFIDENTIAL

treated russet sand pear fruit (Fig 3C). Coincided with this the expression of *PbCER1*, a core component of the complex that controls the biosynthesis of C30 alkanes, was significantly downregulated (Fig 4B). In addition, genes involved in fatty acid elongation, such as *PbKCS19*, *PbKCS10* and *PbKCS20* were also downregulated in the russet fruit (Fig 4).

Therefore, the combined metabolome and transcriptome data analysis indicates that as russeting was intensified in sand pear fruit suberin and related genes were upregulated while the accumulation of long chain fatty acids, waxes and their metabolic genes were suppressed.

As russeting aggravated the primary components of lignin and phenolics in the SL, ferulic acid, epicatechin, and (±)-catechin significantly increased (Table S1). In line with this several recent studies reported that the lignin content was much higher in the peel of the russet than in the green non-russet pear and apple fruit (Wang *et al.*, 2014b, Legay *et al.*, 2015, Shi *et al.*, 2019). Interestingly, we discovered that in the rainfall-treated fruit, higher expression levels were detected for *PbHCT*, *PbCAD1*, *PbCOMT1*, *PbCOMT2*, *PbCCoAOMT* and *PbLAC*, genes encoding for key enzymes in the biosynthesis of lignin monomer phenylpropane. Further, genes encoding for PODs (Q9FLC0, Q42578), the key enzymes for the final step of lignin biosynthesis were also significantly upregulated whilst the expression of *PbCAD6* and *PbCCRSNL-6-like* isoform X2 were severely suppressed in the russet and semi-russet pears (Fig 4B). Suppressing CAD and CCR may cause loosening of the lignin monomer (Bernards and Mark (2002). Therefore, we speculate that there may be two metabolic branches in lignin biosynthesis in russeting in sand pear fruit where *PbCAD1* attributes to the biosynthesis of lignin monomers, whilst *PbCAD6* and *PbCCRSNL-6-like* isoform X2 participate in loosening the lignin structure (Kaur *et al.* (2012). Together they may be beneficial for the fatty substances and lignin monomers biosynthesis and polymerization into suberin, hence promoting russeting in sand pear fruit.

SUBMITTED MANUSCRIPT

Damage caused by long-term rainfall induces an anoxic environment in plants and causes rapid expansion and rupture of the outer epidermal cells. The loosening of cell walls is the pre-requisition for cell expansion which in turn can cause russeting. Our transcriptomics analysis revealed that genes encoding for expansin, including *PbExpA7*, *PbExpA4*, *PbExpA6* and *PbExpB15* all showed much higher expression levels in the russet and semi-russet fruit. Further, rainfall treatment resulted in the rupture of the SL structure of the peel, and induction of increase expression levels of those genes encoding for expansin (Fig 4 and Table S2). Therefore, these results imply that expansin is involved in cell wall loosening hence russeting in sand pear fruit which is enhanced by rainfall.

Studies on aquaporins such as PIPs and TIPs indicated that these proteins may regulate the transmembrane transport of water, thereby maintaining water balance in plants especially under stress conditions (Shao *et al.*, 2008). A study showed that under dry conditions, the expression level of *Aquaporin-1* was reduced in the peel of the sand pear fruit, and this was coincided with reduced transpiration and water loss (Wang *et al.*, 2014a). Up-regulation of aquaporin genes such as *PbTIP1-3*, *PbTIP2-1* and *PbPIP2-5* was found in the rainfall-treated russet and semi-russet sand pear fruit (Fig 4 and Table S2). Therefore, it appears that both expansins and aquaporins were upregulated and involved in rainfall aggravated russeting by loosening cell walls and transmembrane transporting water in sand pear fruit.

Transmembrane transport of cutin and wax to the cell wall is important for the synthesis and deposition of SC. Non-specific lipid transfer proteins (nsLTPs) in Arabidopsis and rice were thought to be involved in cutin and wax synthesis processes (Edstam *et al.*, 2013). The results showed that the expression of nsLTPs protein *and PbnsLTPs* genes were higher in the no-russet peel than it in the russet- and semi-russet peel from the transcriptome and proteome analyses (Fig 5). It was speculated that nsLTPs can promote the transport of small lipophilic molecules that make up wax and cutin to the outside of the cell membrane so

SUBMITTED MANUSCRIPT

that the integrity of the SC was maintained. Therefore, it seems that russeting is negatively regulated by genes involved in the biosynthesis of long chain fatty acids and waxes in sand pear fruit.

To verify the reliability of our data we tested the relationship between russeting of sand pear fruit and one of the highly expressed genes, *PbHHT1* identified from our RNAseq. High level of its encoded protein, PbHHT1 was also detected in the iTRAQ analysis of the russet fruit (Table 2). The homologous gene of *PbHHT1* was first detected in tobacco and subsequently isolated from suberized potato tuber (Lotfy *et al.*, 1996, Wang *et al* 2020). It plays important roles in russeting by catalyzing the conjugation of ferulic acid and palmitic acid to ω~hydroxypalmitic acid, one of the key steps in the biosynthesis of suberin (Schomburg, D. and Schomburg I 2013, Wei *et al* 2019). Our metabolomics analysis showed that the contents of ferulic acid and palmitic acid as well as 16-feruloyloxypalmitic acid were all much higher in the russet and semi russet pears than the control non-russet fruit (Fig 6). Together, these data imply that *PbHHT1* and its encoded protein PbHHT1 most likely play positive roles in the production of 16-feruloyloxypalmitic acid hence russeting in sand pear fruit.

To test this hypothesis PbHHT1 was transiently overexpressed in the young immature semi-russet CG pear fruit before russeting developed, as well as in the same aged non-russet CY fruit. This resulted in the premature russeting covering the entire area where the bacteria solution spread, which corresponded to the large aniline blue stained suberin observed in the CG peel (Fig 6A). Transient expression of PbHHT1 in the CG fruit caused increased expression of genes related to phenylpropanoid-suberin biosynthesis as revealed by the RNAseq analysis. These include *PbCOMT1* and *Pb4CL* which encodes for the key enzymes caffeic acid 3-O-methyltransferase (COMT) and 4-coumarate-CoA ligase (4CL) for the biosynthesis of ferulic acid and feruloyl-CoA, the intermediates for the rapid biosynthesis of 16-feruloyloxypalmitic acid by HHT1 (Graça et al, 2010). Conversely, downregulation of *PbKCS19*, *PbKCS10*, *PbKCS20*, *PbCER1-like* and

CONFIDENTIAL

PbWSD1-like was detected in the PbHHT1 expressing semi-russet CG fruit whilst no changes were found in the CY fruits. While their upregulation was shown and suggested to promote the integrity of the SC structure and therefore inhibit russeting (Wang et al, 2016), lower activities of these genes could lead to a less intact SC structure, hence russeting as found in the PbHHT1 triggered russeting in the young semi-russet CG fruit (Fig 6).

It is noteworthy that the CG and CY fruit exhibited different degrees of russeting after transiently expressing PbHHT1 where the extent was much higher in the CG than the CY fruit (Fig 6A). Although the content of its catalytic product 16-ferulyloxypalmitate was significantly increased in the peel harbouring the *PbHHT1* construct compared to the empty vector in the non-russet CY fruit it was still much lower than in the EV control CG fruit (Fig 6B). Therefore, it seems that there is a threshold amount of 16-ferulyloxypalmitic acid where once this amount is reached genes in the phenylalanine synthesis pathway can be activated, leading to suberin accumulation and russeting. In addition, it also has the potential to negatively regulate cutin and wax biosynthesis, transport and accumulation hence integrity of SC. Together, this can trigger the formation of suberin hence russeting in sand pear fruit.

Through the multi-omics analysis and transient expression of *PbHHT1* in the peel of russet and non-russet pear fruit we show here that russeting in sand pear is a complex process, involving changes in the expression of multiple genes and proteins participating in the biosynthesis of polyphenolics, fatty acids and other secondary metabolites. This leads to the alteration of the biochemical composition as well as physical appearance (texture and colour) of the fruit. By combining all the data obtained in this study we generated a tentative mechanic model of russeting in sand pear fruit and presented in Figure 8. It shows that the russeting related metabolites are first synthesized in the cytoplasm, transported through the plasma membrane and finally assembled at the cell walls of the cells of the fruit peel. Both the phenylpropanoid

SUBMITTED MANUSCRIPT

CONFIDENTIAL

biosynthesis pathway and the LCFAs-monoacylglyceride (16-feruloyloxypalmitic acid) for surberin biosynthesis pathway are involved. In the phenylpropanoid biosynthesis pathway, L-phenylalanine ammonia-lyase (PAL) catalyzes the removal of ammonia from L-phenylalanine to generate trans-cinnamic acid. This is followed by the action of cinnamate-4-hydroxylase (C4H), 4-coumaric acid:CoA A ligase (4CL), the lignin synthase (HCT), p-coumaryl coenzyme A3-hydroxylase (C3H) and caffeoyl-CoA O-methyltransferase (CCoAOMT) which results in the production of feruloyl-CoA, the substrate for PbHHT1 (ω-hydroxypalmitate-O-feruloyl transferase). PbHHT1 catalyzes the conjugation of ferulic acid and ω~hydroxypalmitic acid to form 16-feruloyloxypalmitic acid. On the other hand, feruloyl-CoA can be further converted by cinnamoyl-CoA reductase (CCR), cinnamyl alcohol dehydroge-nase (CAD) and LAC to create the lignin monomer. Higher transcript levels of *PbHCT*, *PbCAD1*, *PbCOMT1*, *PbCOMT2*, *PbCCoAOMT* and *PbLAC*, as well as high protein level of PbPAL1 were detected in the russet ZS and semi-russet CG and in their rainfall treated fruit than the controls (in red, Fig 8). This is also consistent with the increased content of lignin and p-cinnamic acid detected in our study (Table 1). Upregulation of *BGLU44* (β-Glucosidase) and related metabolites such as coumarine and 3-O-p-trans-coumaroylalphitolic acid in the russeting peel were also detected. On the other hand, in the LCFAs-monoacylglyceride for surberin biosynthesis pathway, the biosynthesis and transporter of the very-long chain alkanes such as triacontane (C30) for stratum corneum-related waxes were suppressed, leading to the SC to form on the cell wall. Long-chain fatty acids such as palmitic acid is converted by long-chain acyl-CoA synthetase (LACS) to produce fatty acyl CoA which is further catalyzed by cytochrome P450 to produce ω-hydroxylated fatty acids (ω-OHs). They are further esterified into the suberin monomer 16-feruloyloxypalmitic acid by the action of HHT1. Subsequently, the suberin monomer /oligomer, lignin monomer and small phenolic molecules are transported out of the PM through the active ABC transporters such as ABCG7, ABCG6 and ABCG15. These molecules are finally assembled into a macromolecular suberin polymer on the cell walls and their

CONFIDENTIAL

accumulation can lead to the russet appearance on the sand pear fruit peel.

High expression levels of *PbP450 86B*, *PbHHT1*, *PbLACS4* and *PbFAR3* were detected in the rainfall enhanced russet peel of the CG and ZS fruit. Further functional verification of *PbHHT1* confirmed its important role in triggering premature russeting in the young semi russet CG pear fruit, demonstrating the positive role of PbHHT1 in suberization of the russetting pear genotypes. This is perhaps because it can 'bridge' the phenylpropanoid biosynthesis pathway and the surberin biosynthesis pathway, and therefore, can alter and coordinate the expression of various genes related to russetting in sand pear fruit.

CONFIDENTIAL

EXPERIMENTAL PROCCEDURES

Plant materials

The pear trees of the russet 'Zaoshengxinshui' (ZS), semi-russet 'Cui guan' (CG) and green non-russet 'Cuiyu' (CY) were grown in the Jinshan Fruit Experiment Station of the Shanghai Academy of Agricultural Sciences (30.7875 N, 121.1438 E), Shanghai county, China. Ten days after full bloom (DAFB) the control non rainfall-treated fruit were wrapped with transparent nano-pore bags to avoid contact with rain. For artificial rainfall treatment (rainfall-treated), fruit was sprayed with water to saturation, once a week. Six fruits from each of the 5 selected pear trees were treated for each genotype. The microenvironments within the bags for the non-rainfall and artificial rainfall-treated fruit were monitored throughout the growth season. No significant difference between them in terms of temperature, humidity and light quality were found (Table S7 & Fig. S10). At 80 DAFB, all the fruit from untreated controls ZS-C, CG-C and CY-C, and rainfall treated ZS-R, CG-R and CY-R were collected, the peel was removed, sliced and immediately frozen in liquid nitrogen in the field. These samples were then transported back to the laboratory in liquid nitrogen and stored at −80°C

until further analysis.

Scanning electron microscopy

To observe the suberin layer formation, the peel (5 mm x 5 mm) was excised from freshly harvested fruit and frozen in a pre-cooled tissue holder with frozen glue in a cryogenic liquid nitrogen slurry at a temperature lower than −143.15°C for rapid freezing. Subsequently, the samples were fixed, observed and images were captured by the quorum 2100 scanning electron microscope cryoscopy (Quorum, England).

Fluorescence microscopy observation of the suberinized fruit peel

Peel slices were placed on the glass slides and soaked in 0.1% berberine hydrochloride solution for 60 minutes. After rinsing with distilled water 0.5% aniline blue was added and the samples were stained for 30 minutes. This was followed by the addition of a mixture of 0.1% $FeCl_3$ and glycerol (volume ratio 1:1). After 5 minutes the samples were observed under UV using a fluorescence microscope (Brundrett et al 1988).

Untargeted metabolomics analysis by LC-MS and GC-MS

To analyze the metabolites the stored frozen peel slices were ground and the metabolites were extracted according to Shi et al (2019). For LC-MS analysis, 60 mg of each sample was used. An ACQUITY UHPLC system (Waters Corporation, Milford, USA) fitted with an ACQUITY UPLC BEH C18 column (1.7 µm, 2.1 x 100 mm) coupled with an AB SCIEX Triple TOF 5600 System (AB SCIEX, Framingham, MA) was used in both electrospray ion (ESI) positive and negative modes. To assess the repeatability, the QC sample (a mixture of an equal volume of each sample) was injected at regular intervals of every 10 samples throughout

SUBMITTED MANUSCRIPT

the analytical run. Metabolite labeling was accomplished using the Human Metabolome Database and LIPID MAPS® Structure Database (LMSD) (Scandiani *et al.*, 2015).

For GC-MS analysis, the 7890B-5977A GC/MSD GC/MSD (Agilent Technologies Inc. CA, USA) fitted with a DB-5MS capillary column (30 m x 0.25 mm x 0.25 μm, Agilent J & W Scientific, Folsom, CA, USA) was used. The carrier gas was high-purity helium, and the flow rate was 1.0 mL/min. The inlet temperature was maintained at 260°C. Metabolites were quantified using the NIST and Fiehn database.

For the identification of differentially expressed metabolites, unsupervised principal component analysis was used to observe the overall distribution among samples and the stability of the analytical process. Supervised projection to latent structure-discriminant analysis (PLS-DA) was carried out to distinguish the overall differences between different samples. A variable importance for the projection (VIP) >1, p value <0.05 were considered as threshold values for the differentially expressed metabolites.

CONFIDENTIAL

Metabolite targeted detection

The target compound (phenolic substances and long-chain/very long fatty acids) in the samples were detected qualitatively and quantitatively by the UPLC-Q-TOF/MS mass spectrometry system (Waters, USA) equipped with an electrospray ion (ESI) source and UNIFI 1.8.1 workstation.

RNA-seq analysis

Total RNA was extracted from the pear peel slices and a library was prepared according to the Illumina standard instructions (TruSeq Stranded RNA LT Guide). The raw reads were filtered by Seqtk before mapping

to the pear genome using TopHat (version: 2.0.9). The gene fragments were counted using HTSeq followed by trimmed mean of M (TMM) values normalization (Anders *et al.*, 2014). Significantly differentially expressed genes (DEGs) were identified as those with a false discovery rate (FDR) value above the threshold (Q<0.05) and fold change >2 calculated using the edgeR software. The identities of these DEGs were confirmed by gene ontology (GO) using the Kyoto Encyclopedia of Genes and Genomes (KEGG) enrichment (Ashburner *et al.*, Ogata *et al.*, 1999).

Proteomics by iTRAQ and LC−MS/MS

Total proteins were extracted from the stored fruit peel and digested with trypsin (protein:trypsin, 30:1) at 37°C for 16 hours, as described by Zhao *et al.* (2015). The peptides were desalted and labeled with the 8-plex iTRAQ reagents according to the manufacturer's protocols (AB SCIEX, Framingham, MA, USA). The iTRAQ reagents had molecular masses of 113 (CG-R) and 114 (CG-C) for the rainfall-treated and non-treated control semi-russet CG fruit; 115 (ZS-R) and 116 (ZS-C) for the rainfall-treated and non-treated control russet ZS fruit; and 119 Daltons for the QC (QC mixture), respectively.

For LC−MS/MS analysis, the parameters and methods were carried out as described by Fu *et al* (2015). Subsequently, the data was analyzed for protein identification and quantification using Protein Pilot Software v.5.0 (Sciex Inc., USA). Those proteins identified at global FDR ≤ 1% and unique peptides ≥ 1 were selected for further downstream analysis. The differentially expressed proteins (DEPs) were identified as those with *p*-values < 0.05 and fold change ≥1.2 between different treatments. They were further analyzed using Proteome Discoverer TM 2.2 software (Thermo Corporation, USA) and searched against the pear genome database in NCBI (LM07171185NCBI-Pyrus pear. fasta). Finally, the identified DEPs were annotated with GO terms and

SUBMITTED MANUSCRIPT

CONFIDENTIAL

KEGG enrichment analysis.

Targeted analysis by parallel reaction monitoring (PRM)

The sample preparation for PRM was carried out using the method described by Martinez *et al* (2017). Proteins were digested and desalted by a C18-Reverse-Phase SPE Column and the iRT standard peptides were dissolved in a relative buffer according to the manufacturer's protocol (2xiRT Kit Quick Reference Card). PRM analysis was performed with a Q-Executive Plus mass spectrometer (Thermo Fisher Scientific, San Jose, CA). The original offline files were imported into Proteome Discover 2.3 software to search the pear genome sequence database (LM07171185NCBI-Pyrus pear. fasta). Using Skyline software, the target peptide lists were selected from the data dependent acquisition (DDA) results and imported into the inclusion list of the Xcalibur PRM method editing module. The results were imported into the Skyline software. The actual and the relative retention time, i.e., iRT of the standard peptides were derived from the combined data from statistics (Excel), the Graphpad Prism 8.0 software, the retention time distribution and the correlation with the theoretical retention time (Table S4) (MacLean et al., 2010). Very small deviations between all the standard peptides (11/11) were detected (Fig. S6). The correlation coefficient (R^2) between the actual and theoretical retention time was 0.9986, indicating data were reliable (Fig. S7).

Integration analysis of transcriptome, proteome, and metabolome profiles

The data from the transcriptome, proteome and metabolome were integrated and analyzed in order to identify the key genes, proteins and metabolites that are involved in the common or unique pathways. ID conversion was used to convert genes, proteins and metabolite IDs into the KEGG format (Tables S5, and S6). The IDs were then simultaneously mapped to the KEGG database through GENMAPP. Protein-pathway and protein-

CONFIDENTIAL

protein correlations were obtained, and the network maps were drawn using Cytoscape V3.6.1 bioinformatics analysis software.

Expression analysis by quantitative real-time PCR (qRT-PCR)

Total RNA was extracted from the pear peel using the Plant RNA Preparation Kit (Omega Bio-Tek, Guangzhou, China). The first strand cDNA was synthesized using a Revert Aid First Strand cDNA Synthesis kit (Takara RRO47) and used as templates for real-time PCR as described previously (Shi *et al,* 2019).

***PbHHT1* cloning, vector construction and transient expression in pear fruit**

The coding region of *PbHHT1* (GenBank accession 103966555) was amplified using the primer pair CZ-HHT1-BamHI-F 5'-**ATGTCTAGACTCGAG**ATGGTTGCTGAATTCGGAG-3' and CZ-HHT1-BamHI-R 5'-**AGCCTGCAGCCATGG**CTAGACGTTCATCAGTTCTTG-3'(adaptor sequences for seamless cloning are in bold). The PCR product was verified by gel electrophoresis and purified (Fig. S8). This was followed by recombination into the plant expression vector pCambia 2301 using the ClonExpress II One Step Cloning Kit (https://www.vazymebiotech.cn/) (Fig. S9). The success of cloning was subsequently confirmed by sequencing.

The recombinant pCambia2301-PbHHT1 (PbHHT1) and the pCambia2301 empty vectors (EV) were independently transformed into the Agrobacterium strain GV3101 and a single transgenic colony was inoculated and cultured in LB medium containing kanamycin (50μg/ml), ampicillin (100μg/ml), rifampicin (50μg/ml) and gentamycin (25μg/ml) with shaking at 28°C for 24 hours. The cells were collected by

SUBMITTED MANUSCRIPT

centrifugation and resuspended in the infiltration buffer (10 mM $MgCl_2$, 10 mM MES at pH 5.5 and 20 mM acetosyringone) (MMA). The final OD600 of the bacterial solution was adjusted to ~1.0 and injected into 1-mm below the peel of the young green pear fruit as described by Zhai *et al.* (2016). Those fruit injected with empty vector containing bacteria solution (EV), MMA and water were used as negative controls. The fruit was harvested thirteen days after injection when russet spots appeared. The peel around the injection sites covering the entire bacteria spreading areas was excised, frozen in liquid N_2 and stored in -80°C for the analysis of metabolites and RNAseq (Wu *et al,* 2019).

Statistical analyses

The content of various metabolites and the quantitative expression of DEGs, DEPs and DEMs were analyzed by univariate statistical analysis and presented as the mean ± standard deviation (SD). Significant differences were analyzed using a one-way analysis of variance (ANOVA) and the least significant difference (LSD) multiple range tests was carried out using SPSS 17.0 software (IBM, Armonk, NY, USA). A $p < 0.01$ indicates a statistically significant difference between treatments.

CONFIDENTIAL

ACKNOWLEDGEMENTS

The authors would like to thank the Research and Demonstration of High-efficiency Production Technology in Green Pear Orchard, China (SAS2019 1-3 to JL). We thank Dr. Rachael Symonds of Liverpool John Moores University, UK for English editing this manuscript.

AUTHOR CONTRIBUTIONS

YZ, JL, CS and BQ initiated and designed the project. CS, XW and JX performed and acquired experiments. CS and BQ analyzed and interpreted the data. CS and BQ wrote the manuscript. All authors read and approved the final manuscript for submission.

CONFLICT OF INTEREST

All authors declare that they have no competing interests.

SUPPORTING INFORMATION

Additional Supporting Information may be found in the online version of this article.

Table S1. Overlapped differentially expressed metabolites identified from the rainfall treated and non-treated russet 'Zaoshengxinshui' (ZS), semi-russet 'Cuiguan' (CG) and green non-russet 'Cuiyu' (CY) pear fruit.

Table S2. Overlapped differentially expressed genes identified from the rainfall treated and non-treated russet 'Zaoshengxinshui' (ZS), semi-russet 'Cuiguan' (CG) and green non-russet 'Cuiyu' (CY) pear fruit.

Table S3. Differentially expressed proteins related to russeting by iTRAQ analysis.

Table S4. The retention time (iRT) of the internal peptide standards used in data dependent acquisition (DDA).

Table S5. ID conversion to genes and proteins identified from the rainfall treated and non-treated semi-russet 'Cuiguan' CG.

SUBMITTED MANUSCRIPT

CONFIDENTIAL

Table S6. ID conversion to genes and proteins identified from the rainfall-treated and non-treated russet 'Zaoshengxinshui' ZS fruit peel.

Table S7. Measurements of the photosynthetically active radiation and illuminance (PAR) in the nanopore bags of the control and non-bagged rainfall-treated pear.

Fig. S1. The russet index and cork layer thickness of the russet 'Zaoshengxinshui' (ZS), semi-russet 'Cuiguan' (CG) and green non-russet 'Cuiyu' (CY) (control). R, rainfall-treated fruit, C, non-rainfall-treated control fruit, DAFB, day after full bloom. The data are represented as the mean ± standard deviation (n = 9). ** $p < 0.01$.

Fig. S2. Principal Component Analysis (PCA) of differentially expressed metabolites (DEMs) in the peel of russet 'Zaoshengxinshui' (ZS), semi-russet 'Cuiguan' (CG) and green non-russet 'Cuiyu' (CY) fruit.

(a) PCA of DEMs of ZS, CG and CY fruit by Liquid chromatography-tandem mass spectrometry (LC-MS).

(b) PCA of DEMs of ZS, CG and CY fruit by Gas chromatography–mass spectrometry (GC-MS).

R, rainfall-treated fruit, C, non-rainfall-treated control fruit.

Fig. S3. Absolute quantification of DEMs related to the suberin lamellae in the peel of rainfall-treated (R) and non-treated control (C) ZS, CG and CY fruit.

Fig. S4. KEGG enrichment of DEGs in the peel of ZS, CG and CY, as well as in the rainfall-treated (R) and non-treated control (C) of the russet ZS and semi-russet CG fruit.

Fig. S5. Venn diagrams to show DEGs that are common between ZS, CG and CY as well as between the rainfall-treated (R) and non-treated control (C) ZS and CG fruit.

CONFIDENTIAL

Fig. S6. The eleven standard peptides and their retention time.

Fig. S7. The correlation between the measured and the theoretical values of the retention time (iRT) of the internal standard peptides by regression analysis.

Fig. S8. PCR amplification of the coding region of *PbHHT1* from the semi-russet 'Cuiguan' (CG) pear fruit.

Fig. S9. Map of the *PbHHT1* plant expression vector used for transient expression in the young green pear fruit.

Fig. S10. Temperature and humidity in in the nanopore bags of the control and non-bagged rainfall-treated fruit.

CONFIDENTIAL

REFERENCES

Anders, S., Pyl, P.T. and Huber, W. (2014) HTSeq—a Python framework to work with high-throughput sequencing data. *Bioinformatics*, **31**, 166-169.

Ashburner, M., Ball, C.A., Blake, J.A., Botstein, D., Butler, H., Cherry, J.M., Davis, A.P., Dolinski, K., Dwight, S.S. and Eppig, J.T. Gene Ontology: tool for the unification of biology. Nat Genet, **25**, 25-29.

Barberon, M., Vermeer, J.E.M., DeBellis, D., Wang, P., Naseer, S., Andersen, T.G., Humbel, B.M., Nawrath, C., Takano, J. and Salt, D.E. (2016) Adaptation of Root Function by Nutrient-Induced Plasticity of Endodermal Differentiation. Cell, **164**, 447-459.

Bernards and Mark, A. (2002) Demystifying suberin. *Can.j.bot*, **80**, 227-240.

Brundrett, M.C., Enstone, D.E., and Peterson, C.A. (1988) A berberine-aniline blue fluorescent staining procedure for suberin, lignin, and callose in plant tissue. Protoplasma, **146**, 133-142.

Cohen, H., Szymanski, J., Aharoni, A. and Dominguez, E. (2017) Assimilation of 'omics' strategies to study the cuticle layer and suberin lamellae in plants. *Journal of Experimental Botany*, **68**, 5389-5400.

Daqiu, Zhao, Saijie, Gong, Zhaojun, Hao, Jiasong, Meng, Jun and Tao (2015) Quantitative Proteomics Analysis of Herbaceous Peony in Response to Paclobutrazol Inhibition of Lateral Branching. *International Journal of Molecular Sciences,* **16**, 24332-24352.

Duan, H., & Schuler, M. A. (2005) Differential expression and evolution of the Arabidopsis CYP86A subfamily. *Plant physiology*, **137**, 1067-1081.**Edstam, M.M., Blomqvist, K., Eklf, A., Wennergren, U. and Edqvist, J.** (2013) Coexpression patterns indicate that GPI-anchored non-specific lipid transfer proteins are involved in accumulation of cuticular wax, suberin and sporopollenin. *Plant Molecular Biology*, **83**, 625-649.

Escamilla-Trevi?o, L.L., Chen, W., Card, M.L., Shih, M.C., Cheng, C.L. and Poulton, J.E. (2006) Arabidopsis thaliana beta-Glucosidases BGLU45 and BGLU46 hydrolyse monolignol glucosides. *Phytochemistry*, **67**, 1651-1660.

Franke, R. and Schreiber, L. (2007) Suberin--a biopolyester forming apoplastic plant interfaces. *Current Opinion in Plant Biology*, **10**, 252-259.

Fu, Y., Zhang, H., Mandal, S.N., Wang, C. and Ji, W. (2015) Quantitative proteomics reveals the central changes of wheat in response to powdery mildew. *Journal of Proteomics*, **130**, 108-119.

Gamble, J., Jaeger, S.R. and Harker, F.R. (2006) Preferences in pear appearance and response to novelty among Australian and New Zealand consumers. *Postharvest Biology & Technology*, **41**, 38-47.

Graça, J. and Santos, S. (2010) Suberin: A Biopolyester of Plants' Skin. *Macromolecular Bioscience*, **7**, 128-135.

Heng, W., Liu, L., Wang, M.D., Jia, B., Liu, P., Ye, Z.F. and Zhu, L.W. (2014) Differentially expressed genes related to the formation of russet fruit skin in a mutant of 'Dangshansuli' pear (Pyrus bretchnederi Rehd.) determined by suppression subtractive hybridization. *Euphytica*, **196**, 285-297.

Hou, Z., Jia, B., Li, F., Liu, P., Liu, L., Ye, Z., Zhu, L., Wang, Q. and Heng, W. (2018) Characterization and expression of the ABC family (G group) in 'Dangshansuli' pear (Pyrus bretschneideri Rehd.) and its russet mutant. *Genetics and Molecular Biology*, **41**, 137-144.

Inoue, E., Kasumi, M., Sakuma, F., Anzai, H., Amano, K. and Hara, H. (2006) Identification of RAPD marker linked to fruit skin color in Japanese pear (Pyrus pyrifolia Nakai). *Scientia Horticulturae*, **107**, 254-258.

Jia, X.M., Zhu, Y.F., Hu, Y., Zhang, R. and Wang, Y.X. (2019) Integrated physiologic, proteomic, and metabolomic analyses of Malus halliana adaptation to saline–alkali stress. *Horticulture Research*, **6**, 91.

Justin, L., Asaph, A. and Fabrizio, C. (2015) Genome investigation suggests MdSHN3, an APETALA2-domain transcription factor gene, to be a positive regulator of apple fruit cuticle formation and an inhibitor of russet development. *Journal of Experimental Botany*, **66**:6579-6589.

Kaur, H., Shaker, K., Heinzel, N., Ralph, J., Galis, I. and Baldwin, I.T. (2012) Environmental stresses of field growth allow cinnamyl alcohol dehydrogenase-deficient Nicotiana attenuata plants to compensate for their structural deficiencies, **159**, 1545-1570

CONFIDENTIAL

Krishnamurthy, P., Ranathunge, K., Nayak, S., Schreiber, L. and Mathew, M.K. (2011) Root apoplastic barriers block Na+ transport to shoots in rice (Oryza sativa L.). *Journal of Experimental Botany*, **62**, 4215-4228.

Lara, I., Belge, B. and Goulao, L.F. (2015) A focus on the biosynthesis and composition of cuticle in fruits. *J Agric Food Chem*, **63**, 4005-4019.

Legay, S., Guerriero, G., Deleruelle, A., Lateur, M., Evers, D., André, C.M. and Hausman, J.-F. (2015) Apple russeting as seen through the RNA-seq lens: strong alterations in the exocarp cell wall. *Plant Molecular Biology*, **88**, 21-40.

Li, A.X., Han, Y.Y., Wang, X., Chen, Y.H., Zhao, M.R., Zhou, S.M. and Wang, W. (2015) Root-specific expression of wheat expansin gene TaEXPB23 enhances root growth and water stress tolerance in tobacco. *Environmental & Experimental Botany*, **110**, 73-84.

Li, Y., Beisson, F., Koo, A.J.K., Molina, I., Pollard, M. and Ohlrogge, J. (2007) Identification of acyltransferases required for cutin biosynthesis and production of cutin with suberin-like monomers. *Proceedings of the National Academy of Sciences of the United States of America*, **104**, 18339-18344.

Lotfy, S., Javelle, F. and Negrel, J. (1996) Purification and characterization of hydroxycinnamoyl- Coenzyme A: ω- hydroxypalmitic acid O-hydroxycinnamoyltransferase from tobacco (Nicotiana tabacum L.) cell-suspension cultures. *Planta*, **199**, 475-480.

MacLean, B., Tomazela, D.M., Shulman, N., Chambers, M., Finney, G.L., Frewen, B., Kern, R., Tabb, D.L., Liebler, D.C. and MacCoss, M.J. (2010) Skyline: an open source document editor for creating and analyzing targeted proteomics experiments. *Bioinformatics*, **26**, 966-968.

Martinez, E., Lesur, A., Devis, L., Cabrera, S., Matias-Guiu, X., Hirschfeld, M., Asberger, J., Van Oostrum, J., Casares de Cal, M.d.l.á. and Gómez-Tato, A. (2017) Targeted proteomics identifies proteomic signatures in liquid-biopsies of the endometrium to diagnose endometrial cancer and assist in the prediction of the optimal surgical treatment. *Clinical Cancer Research An Official Journal of the American Association for Cancer Research*, clincanres,**23**:6458-6467.

Norris, R.F. and Bukovac, M.J. (2010) Influence of cuticular waxes on penetration of pear leaf cuticle by 1-naphthaleneacetic acid. *Pest Management Science*, **3**, 705-708.

Ogata, H., Goto, S., Sato, K., Fujibuchi, W., Bono, H. and Kanehisa, M. (1999) KEGG: Kyoto Encyclopedia of Genes and Genomes. *Nucleic Acids Res*, **27**, 29-34.

Perez-Enciso, M., Toro, M.A., Tenenhaus, M. and Gianola, D. (2003) Combining gene expression and molecular marker information for mapping complex trait genes: a simulation study. *Genetics*, **164**, 1597-1606.

Pollard, M., Beisson, F., Li, Y. and Ohlrogge, J.B. (2008) Building lipid barriers: biosynthesis of cutin and suberin. *Trends Plant Sci*, **13**, 236-246.

Riederer, M. and Schreiber, L. (2001) Protecting against water loss: analysis of the barrier properties of plant cuticles. *J Exp Bot*, **52**, 2023-2032.

Scandiani, M.M., Luque, A.G., Razori, M.V., Lucila, C.C., Takayuki, A., Kerry, O.D., Cervigni, G.D.L. and Spampinato, C.P. (2015) Metabolic profiles of soybean roots during early stages of Fusarium tucumaniae infection. *Journal of Experimental Botany*, 391.

Secchi, F., Pagliarani, C. and Zwieniecki, M.A. (2017) The functional role of xylem parenchyma cells and aquaporins during recovery from severe water stress. *Plant Cell & Environment*, **40**, 858-871.

Serra, O., Chatterjee, S., Figueras, M., Molinas, M. and Stark, R.E. (2014) Deconstructing a plant macromolecular assembly: chemical architecture, molecular flexibility, and mechanical performance of natural and engineered potato suberins. *Biomacromolecules*, **15**, 799-811.

Shao, H.B., Chu, L.Y., Shao, H.B., Chu, L.Y., Shao, M.A. and Zhao, C.X. (2008) Advances in functional regulation mechanisms of plant aquaporins: Their diversity, gene expression, localization, structure and roles in plant soil-water relations (Review). *Molecular Membrane Biology*, **25**, 179-191.

Schomburg, D., and Schomburg I . (2013). ω-hydroxypalmitate o-feruloyl transferase 2.3.1.188. Springer Berlin Heidelberg.

Shi, C.H., Qi, B.X., Wang, X.Q., Sheng, L.Y., Luo, J. and Zhang Y.X. (2019) Proteomic analysis of the key mechanism of exocarp russet pigmentation of semi-russet pear under rainwater condition. *Scientia Horticulturae*, **254**, 178-186.

CONFIDENTIAL

Vishwanath, S.J., Delude, C., Domergue, F. and Rowland, O. (2015) Suberin: biosynthesis, regulation, and polymer assembly of a protective extracellular barrier. *Plant Cell Rep*, **34**, 573-586.

Wang, G., Xu, J., Li, L., Guo, Z., Si, Q., Zhu, G., Wang, X., and Guo W. (2019) GbCYP86a1-1 from gossypium barbadense positively regulates defence against Verticillium dahliae by cell wall modification and activation of immune pathways. *Plant Biotechnology Journal,* **18**.

Wang, Y.Z., Dai, MS., Zhang, S.J. and Shi, Z.B. (2014a) Exploring Candidate Genes for Pericarp Russet Pigmentation of Sand Pear (Pyrus pyrifolia) via RNA-Seq Data in Two Genotypes Contrasting for Pericarp Color. *Plos One*, **9,** .e83675.

Wang, Y.Z., Dai, M.S., Cai, D.Y. and Shi, Z.B (2020) Proteome and transcriptome profile analysis reveals regulatory and stress-responsive networks in the russet fruit skin of sand pear. *Horticulture Research*, **7**, 16.

Wang, Y.Z., Dai, M.S., Cai, D.Y., Zhang, S. and Shi, Z.B. (2016) A review for the molecular research of russet/semi-russet of sand pear exocarp and their genetic characters. *Scientia Horticulturae*, **210**, 138-142.

Wang, Y.Z., Zhang, S., Dai, M.S. and Shi, Z.B. (2014b) Pigmentation in sand pear (Pyrus pyrifolia) fruit: biochemical characterization, gene discovery and expression analysis with exocarp pigmentation mutant. *Plant Molecular Biology*, **85**, 123-134.

Wei, X., Lu, W., Mao, L., Han, X., and Xu, C. (2019). ABF2 and MYB transcription factors dominate feruloyl transferase fht gene involved in aba-mediated wound suberization of kiwifruit. *Journal of Experimental Botany*, **71**, 305-317.

Wu, M., Si, M., X.Li, Song, L.Y, Liu, J.L., Zhai, R., Cong, L., Yue, R.R., Yang C.Q., Ma, F.W., Xu, L.F. and Wang Z.G. (2019). Pbcop1.1 contributes to the negative regulation of anthocyanin biosynthesis in pear. *Plants*, **8**, 39.

Zhai, R., Wang, Z., Zhang, S., Meng, G., Song, L., Wang, Z., Li, P., Ma, F. and Xu, L. (2016) Two MYB transcription factors regulate flavonoid biosynthesis in pear fruit (Pyrus bretschneideri Rehd.). *J Exp Bot*, **67**, 1275-1284.

CONFIDENTIAL

Table 1. The overlapping differentially expressed genes (DEGs) related to the biosynthesis of cutin, suberin and wax identified between the russet 'Zaoshengxinshui' (ZS) and green non-russet 'Cuiyu' (CY) (ZS vs CY); semi-russet 'Cuiguan' (CG) and green non-russet CY (CG vs CY); rainfall-treated (R) and non-treated (C) russet ZS (ZS (R vs C), and rainfall-treated (R) and no-rainfall-treated (C) of semi-russet CG (CG (R vs C) pear fruit.

Plus values indicate upregulation, minus ones downregulation. ZS vs CY, between the russet 'Zaoshengxinshui' (ZS) and green non-russet 'Cuiyu' (CY); CG vs CY, between the semi-russet 'Cuiguan' (CG) and CY; ZS (R vs C), between rainfall-treated and non-rainfall-treated russet ZS; CG (R vs C), between rainfall-treated (R) and non-rainfall-treated (R) russet CG pear fruit.

Acc. no.	Gene name	Description	Log_2(FC)			
			ZS vs CY	CG vs CY	ZS (R vs C)	CG (R vs C)
103966555	*PbHHT1-like*	PREDICTED: omega-hydroxypalmitate O-feruloyl transferase-like	+2.65	+3.68	+0.21	+3.21
103948102	*PbCYP749A22-like*	PREDICTED: cytochrome P450 CYP749A22-like	+5.10	+3.45	+1.10	--
103949661	*PbKCS10-like*	PREDICTED: 3-ketoacyl-CoA synthase 10-like	-8.15	-3.43	-1.36	-2.94
103943280	*PbCCR SNL6-like*	PREDICTED: cinnamoyl-CoA reductase-like SNL6 isoform X1	-5.57	-3.35	-1.07	-2.76
103928845	*PbWSD1-like*	PREDICTED: O-acyltransferase WSD1-like	-7.18	-3.67	-1.79	-2.89
103929753	*PbCER1-like*	PREDICTED: protein ECERIFERUM 1-like isoform X1	-5.86	-3.07	-1.83	-4.65
103934278	*PbABCG10*	PREDICTED: ABC transporter G family member 10-like	+2.85	+3.31	+1.12	+4.62
103963796	*PbABCG15*	PREDICTED: ABC transporter G family member 15-like	-8.25	-3.16	-1.82	-3.45
103942099	*PbABCG15*	PREDICTED: ABC transporter G family member 15-like	-5.26	-3.44	-2.21	-3.09
103955899	*PbABCG15*	PREDICTED: ABC transporter G family member 15-like	-7.15	-2.69	-3.28	-2.98
103961207	*PbnsLTP-like*	PREDICTED: non-specific lipid-transfer protein-like	-5.86	-3.53	-1.30	-3.26
103938613	*PbnsLTP*	PREDICTED: non-specific lipid-transfer protein	-7.16	-4.09	-2.17	-3.23
103961206	*PbnsLTP*	PREDICTED: non-specific lipid-transfer protein	-6.99	-3.65	-1.78	-3.20

CONFIDENTIAL

Table 2. Top hits of common DEGs and DEPs identified from RNA-seq and iTRAQ analysis of different samples. Plus values indicate upregulation, minus ones downregulation. ZS vs CY, between the russet 'Zaoshengxinshui' (ZS) and green non-russet 'Cuiyu' (CY); CG vs CY, between the semi-russet 'Cuiguan' (CG) and green non-russet 'Cuiyu' (CY); ZS (R vs C), between rainfall-treated (R) and non-rainfall-treated (C) russet ZS; CG (R vs C), between rainfall-treated (R) and non-rainfall-treated (C) semi-russet CG pear fruit.

Acc. no. (gene)	Acc. no. (protein)	Description	$Log_{1.2}$(FC) (protein)				$Log_{2.0}$(FC) (gene)			
			ZS vs CY	CG vs CY	ZS (R vs C)	CG (R vs C)	ZS vs CY	CG vs CY	ZS (R vs C)	CG (R vs C)
103966555	694406379	PREDICTED: omega-hydroxypalmitate O-feruloyl transferase-like [Pyrus x bretschneideri]	+1.69	+4.48	+4.35	+4.10	+2.65	+3.68	+0.21	+3.21
103952998	694312604	PREDICTED: 3-ketoacyl-CoA synthase 10-like [Pyrus x bretschneideri]	+0.41	-1.16	-2.30	-1.77	-5.23	-7.86	-4.34	-0.79
103938613	694440153	PREDICTED: non-specific lipid-transfer protein [Pyrus x bretschneideri]	-0.41	-4.06	-8.54	-7.57	-7.16	-4.09	-2.17	-3.23
103961207	694393124	PREDICTED: non-specific lipid-transfer protein-like [Pyrus x bretschneideri]	-0.21	-4.66	-7.78	-6.66	-5.86	-3.53	-1.30	-3.26

FIGURE LEGENDS

Figure 1. Phenotypic difference between the russet 'Zaoshengxinshui' (ZS), semi-russet 'Cuiguan' (CG) and green non-russet 'Cuiyu' (CY), and between the rainfall treated and non-treated russeting of ZS and CG fruit.

A. Phenotypic difference between ZS, CG and CY pear fruit. Left panel, images of the whole fruit; middle panel, scanning electron microscopy observation of the fruit surface; right panel, transmission electron microscopy observation of the fruit peel. SL, Suberin lamella; SC, stratum corneum; CW, cell wall; Tc, tannin cells; LAMB, liposomes; Cu, cutin layer; Chl, chloroplast; V, vacuole.

B. Effect of rainfall on russetting of russet ZS (top) and semi-russet CG (bottom) pear fruit. Left panel, non-rainfall-treated control fruit; right panel, rainfall-treated fruit.

C. Scanning electron microscopic images of the surface of pear fruit. Left panel, control, non-rainfall treated fruit; right panel, rainfall-treated fruit. SL, suberin lamella; SC, stratum corneum; CW, cell wall; Tc, tannin cells; LAMB, liposomes; Cu, cutin layer.

D. The different russet index between the three different pear genotypes. ZS, 'Zaoshengxinshui' (russet); CG 'Cuiguan' (semi-russet); CY, **'**Cuiyu' (non-russet). Data are expressed as the means ± SD of three biological replicates. $^{**}p < 0.01$.

E. The effect of artificial rainfall treatment on the russet index of the semi-russet CG pear fruit. R, rainfall-treated, C, non-rainfall treated controls. Data are expressed as the means ± SD of three biological replicates. $^{**}p < 0.01$.

F. The effect of rainfall treatment on the thickness of suberin lamellae of ZS pear fruit. R, rainfall-treated, C, non-rainfall-treated controls. Data are expressed as the means ± SD of three biological replicates. $^{**}p < 0.01$

Figure 2. KEGG enrichment of the differentially expressed metabolites (DEMs) obtained from the LC-MS analysis of the russet 'Zaoshengxinshui' (ZS), semi-russet 'Cuiguan' (CG) and non-russet 'Cuiyu' (CY), and from the artificial rainfall-treated ZS and CG sand pear fruit.

A. Bubble diagram of the KEGG enrichment of DEMs from ZS, CG and CY fruit.

B. Bubble diagram of the KEGG enrichment of DEMs related to russeting of the rainfall-treated (R-) and non-treated control (C-) ZS and CG fruit.

Figure 3. Differentially expressed metabolites (DEMs) by LC-MS between the russet 'Zaoshengxinshui' (ZS), semi-russet 'Cuiguan' (CG) and green non-russet 'Cuiyu' (CY), and from the rainfall-treated ZS and CG sand pear fruit.

A. Heatmaps of DEMs related to russeting between the three different pear genotypes of ZS, CG and CY fruit (n=8) (top), and between the rainfall-treated (R) and non-treated control (C) ZS and CG fruit (bottom) (n=8).

B. Venn diagrams to identify overlapping DEMs between ZS, CG and CY, and between the rainfall-treated (R) and non-rainfall-treated control (C) ZS and CG fruit.

CONFIDENTIAL

C. Core russeting related DEMs between the ZS, CG and CY, and between the rainfall-treated (R) and non-rainfall-treated ZS and CG control (C) fruit. Enhanced DEMs are indicated in red and inhibited DEMs in green.

Figure 4. Differentially expressed genes (DEGs) by RNA-seq analysis between russet 'Zaoshengxinshui' (ZS), semi-russet 'Cuiguan' (CG) and green non-russet 'Cuiyu' (CY), and between the rainfall treated and non-treated ZS and CG fruit.

A. Heatmap of russeting related DEGs between ZS, CG and CY, and between the rainfall-treated (R) and non-rainfall-treated control (C-) of ZS and CG fruit.

B. Transcript abundance of DEGs related to russeting in the peels of ZS, CG and CY fruit.

C. Transcript abundance of DEGs related to russeting in rainfall-treated (R) and non-rainfall treated control (C) of ZS and CG sand pear fruit (n = 3). The data are represented as the means ± standard deviation. ** $p <$ 0.01.

Figure 5. Parallel Reaction Monitoring (RPM) identification of russeting related core proteins of absolute abundance in the peels of the rainfall-treated (R) and non-treated control (C) of ZS and CG sand pear fruit. The data are represented as the mean ± standard deviation. * $p< 0.05$. ** $p < 0.01$.

Figure 6. Transient expression of *PbHHT1* triggered russeting in the green young non russet of CG (semi-russet) and the green CY (non-russet) pear fruit.

A. Transient expression of *PbHHT1* in CG and CY fruit. Observation was made 13 days after injection of transgenic Agrobacteria GV3101 harbouring the 35S:PbHHT1 construct. The russet spot around the injection site was clearly seen. Top panel, images of the whole fruit. The entire part of the russeting in the *PbHHT1* expressing CG fruit is marked with a yellow dotted line box while the injection sites with red circles. Bottom panel, fluorescence microscopy observation of the stained peel by aniline blue. Arrows indicate aniline blue stained suberin. PbHHT1, PbHHT1 containing agrobacteria; EV, empty vector containing agrobacteria; MMA, the infiltration buffer (10 mM $MgCl_2$, 10 mM MES at pH 5.5 and 20 mM acetosyringone).

B. LC-MS identification and quantification of ω-feruloyloxypalmitic acid.

C. Expression level of *PbHHT1* by qRT-PCR.

D. The heatmap of DEGs identified by RNAseq from the peel injected with 35S:PbHHT1 (H1) and empty vector (EV) of CG and CY fruit. Statistical significance was determined by the Tukey HSD test (n=5). *p <0.05, **p <0.01.

Figure 7. Integrated network of metabolism of russeting in the rainfall treated russet 'Zaoshengxinshui' (ZS) and semi-russet 'Cuiguan' (CG) sand pear fruit.

A. Russeting metabolism in the rainfall treated russet ZS sand pear fruit.

SUBMITTED MANUSCRIPT

B. Russeting metabolism in the rainfall-treated semi-russet CG sand pear fruit.

The nodes represent omics measurements and edges correlation-based interactions between omics measurements. The five major clusters I–V are represented by different colored block area, I. phenylpropanoid biosynthesis, in blue; II. cutin, suberin and wax biosynthesis, in green; III. fatty acid metabolism, in pink; IV, flavonoid biosynthesis, in purple and V. fatty acid elongation, in yellow. Circles represent genes/proteins, squares signal pathways, triangle arrows metabolic metabolites. Map node size represents the degree that is the most direct measurement to describe the node centrality in the network analysis. The larger and darker the node size the higher the degree centrality of the node.

Figure 8. Proposed model of russeting in sand pear fruit.

Russeting was attributed by both the PAL (Phenylalanine ammonia lyase) phenylpropanoid lignin biosynthesis pathway and the LCFAs (Long-chain fatty acids)-monoacylglyceride (16-feruloyloxypalmitic acid) for suberin biosynthesis pathway. The involvement of the phenylpropanoid biosynthesis pathway was evidenced by the increased content of lignin, p-cinnamic acid and the catalytic products, coumarine and 3-O-p-trans-Coumaroylalphitolic acid of BGLU (β-Glucosidases). On the other hand, the biosynthesis and transportation of very-long chain alkanes (triacontan, C30) of stratum corneum related waxes were suppressed. Subsequently, the suberin monomer /oligomer, lignin monomer and small phenolic molecules were transported out of the membrane by the active ABC transporters where they were polymerized by the polyester synthases (PS) and finally assembled into a macromolecular suberin polymer on the cell wall. Its accumulation leads to russeting on the peel of sand pear fruit. Note that PbHHT1 plays important roles by acting as a 'bridge' between the phenylpropanoid lignin biosynthesis and the LCFAs-monoacylglyceride for suberin biosynthesis pathways.

HHT1, ω-hydroxypalmitate-O-feruloyl transferase; COMT, caffeic acid 3-O-methyltransferase; 4CL, 4-coumarate-CoA ligase; PAL, L-phenylalanine ammonia-lyase; C4H, cinnamate-4-hydroxylase; 4CL, 4-coumaric acid:CoA A ligase; HCT, the lignin synthase; C3H, p-coumaryl coenzyme A3-hydroxylase; CCoAOMT, caffeoyl-CoA O-methyltransferase; CCR, cinnamoyl-CoA reductase; CAD, cinnamyl alcohol dehydroge-nase; LACS, long-chain acyl-CoA synthetase; BGLU44, β-Glucosidase.

Solid dots indicate metabolites, genes and proteins identified in this study where blue dots indicate down-regulation while red up-regulation of DEGs, DEPs and DEMs. Arrows indicate the direction of the pathways where the solid lined arrows indicate the characterized and published whilst the dotted lined arrows the reported yet to be published metabolic pathways on KEEG.

CONFIDENTIAL

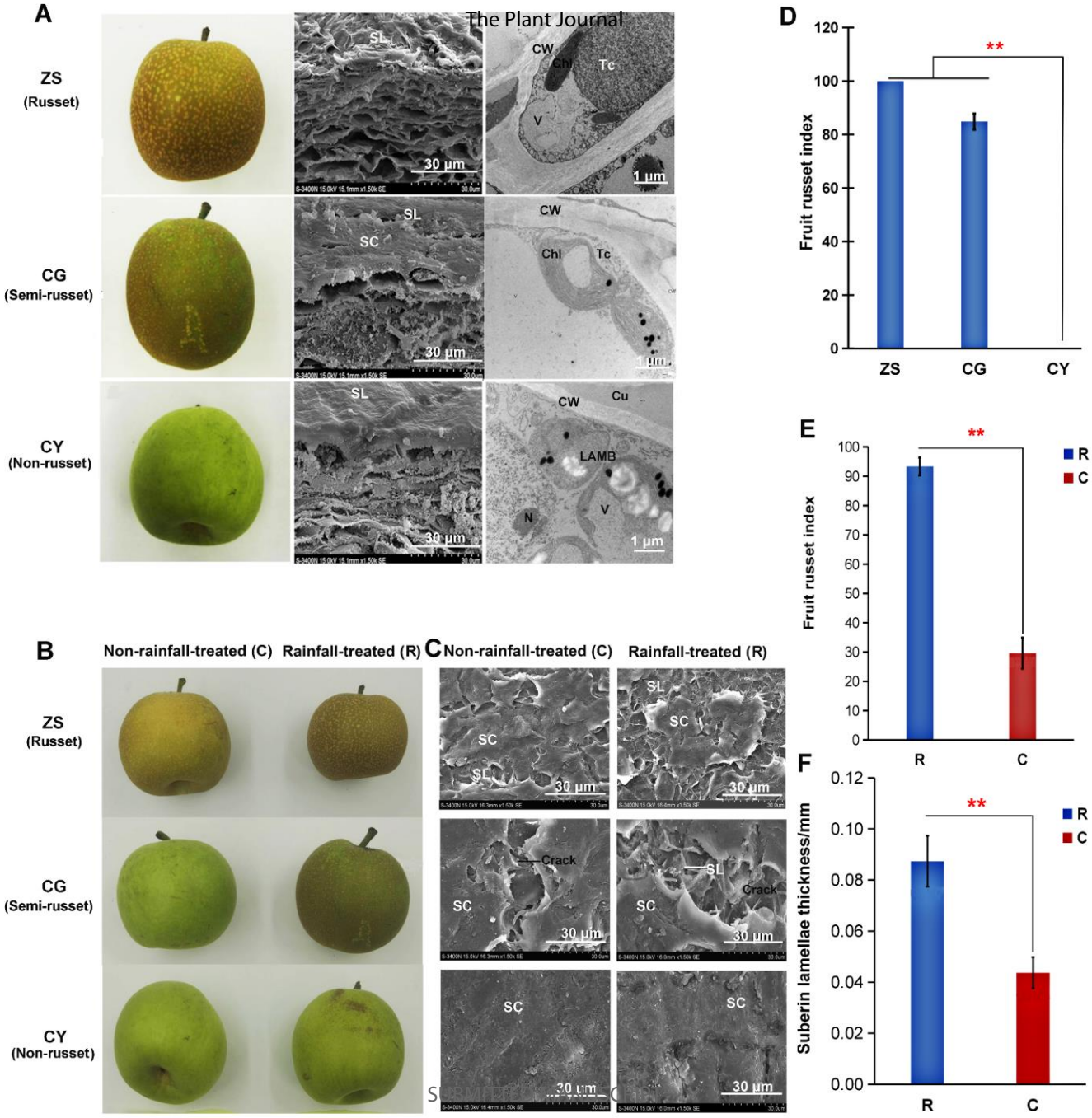
A
ZS
(Russet)
CG
(Semi-russet)
CY
(Non-russet)
SL
SC
CW
Chl
Tc
V
Cu
LAMB
N
30 μm
1 μm
B
Non-rainfall-treated (C)
Rainfall-treated (R)
C
Non-rainfall-treated (C)
Rainfall-treated (R)
Crack
D
Fruit russet index
120
100
80
60
40
20
0
**
ZS
CG
CY
E
Fruit russet index
100
90
80
70
60
50
40
30
20
10
0
**
R
C
F
Suberin lamellae thickness/mm
0.12
0.10
0.08
0.06
0.04
0.02
0.00
**
R
C

Fig 2

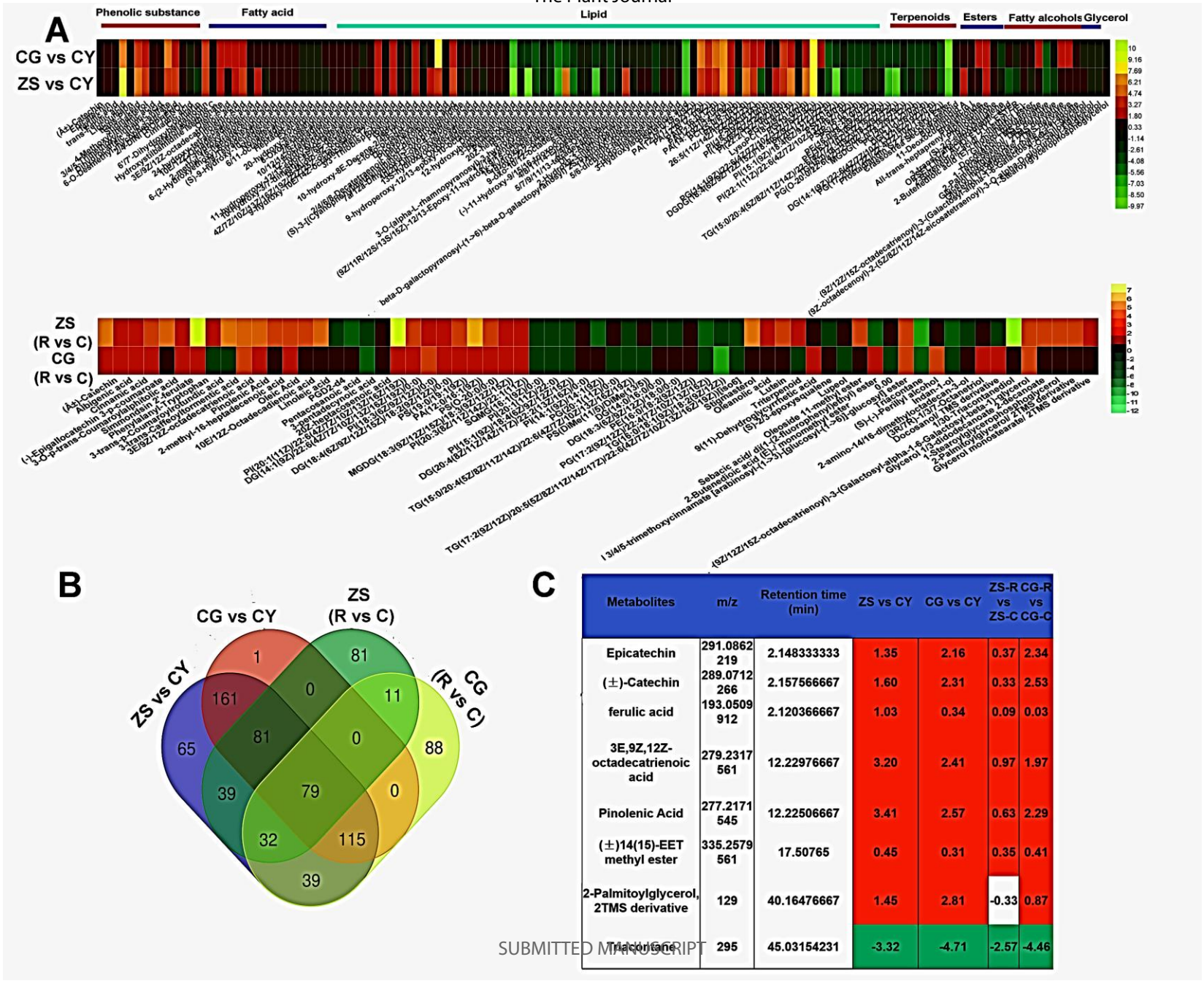

Metabolites	m/z	Retention time (min)	ZS vs CY	CG vs CY	ZS-R vs ZS-C	CG-R vs CG-C
Epicatechin	291.0862219	2.148333333	1.35	2.16	0.37	2.34
(±)-Catechin	289.0712266	2.157566667	1.60	2.31	0.33	2.53
ferulic acid	193.0509912	2.120366667	1.03	0.34	0.09	0.03
3E,9Z,12Z-octadecatrienoic acid	279.2317561	12.22976667	3.20	2.41	0.97	1.97
Pinolenic Acid	277.2171545	12.22506667	3.41	2.57	0.63	2.29
(±)14(15)-EET methyl ester	335.2579561	17.50765	0.45	0.31	0.35	0.41
2-Palmitoylglycerol, 2TMS derivative	129	40.16476667	1.45	2.81	-0.33	0.87
Thalianone	295	45.03154231	-3.32	-4.71	-2.57	-4.46

SUBMITTED MANUSCRIPT

Fig 3

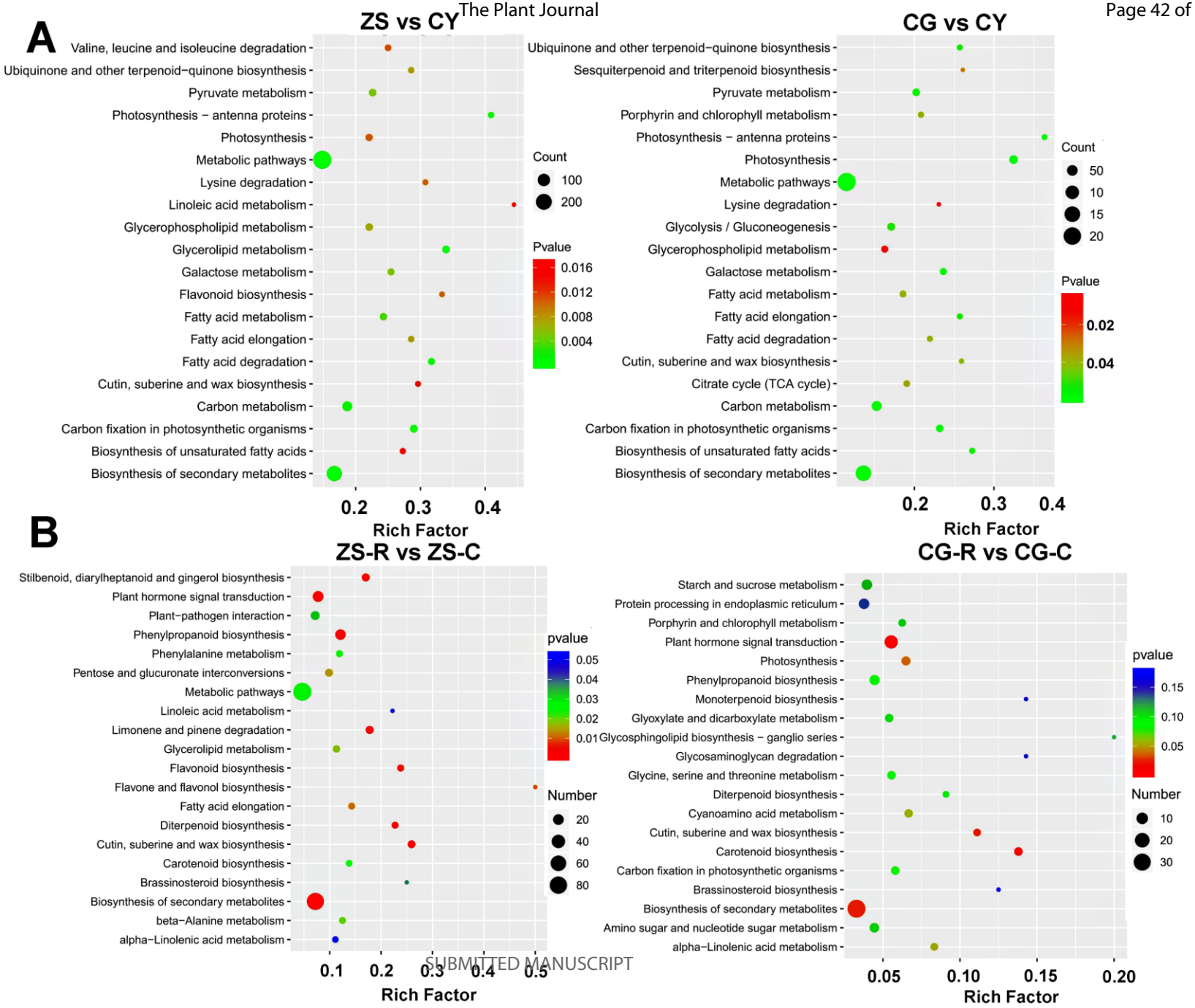

SUBMITTED MANUSCRIPT

Fig 4

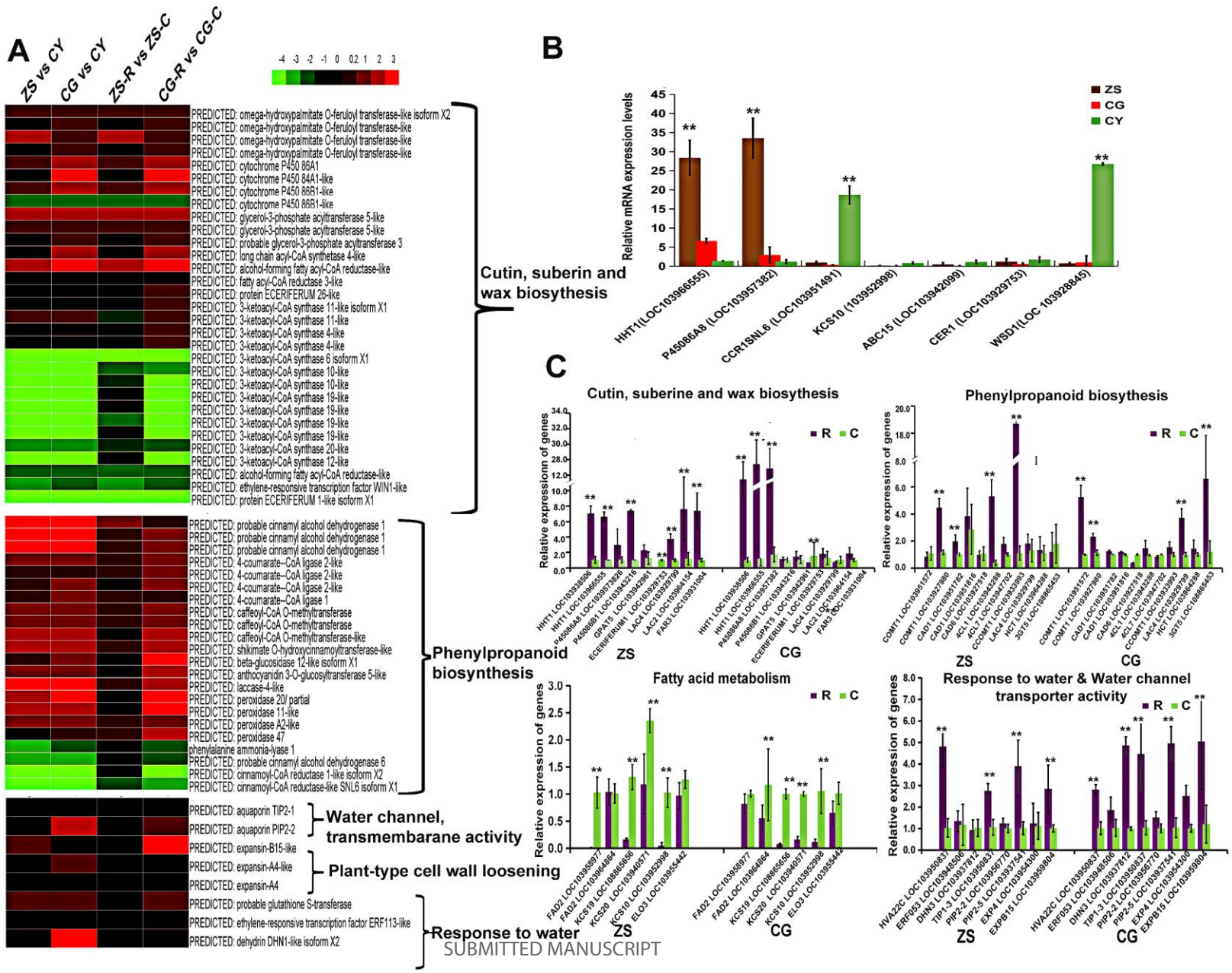

SUBMITTED MANUSCRIPT

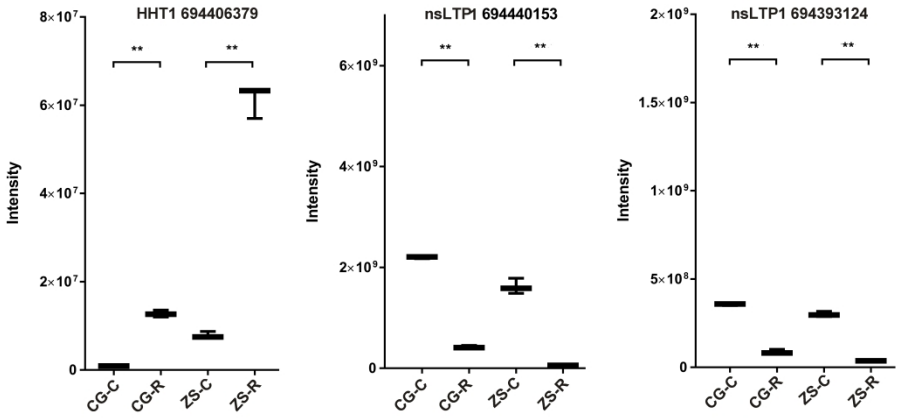

Figure 5. Parallel Reaction Monitoring (RPM) identification of russeting related core proteins of absolute abundance in the peels of the rainfall-treated (R) and non-treated control (C) of ZS and CG sand pear fruit. The data are represented as the mean ± standard deviation. * $p < 0.05$. ** $p < 0.01$.

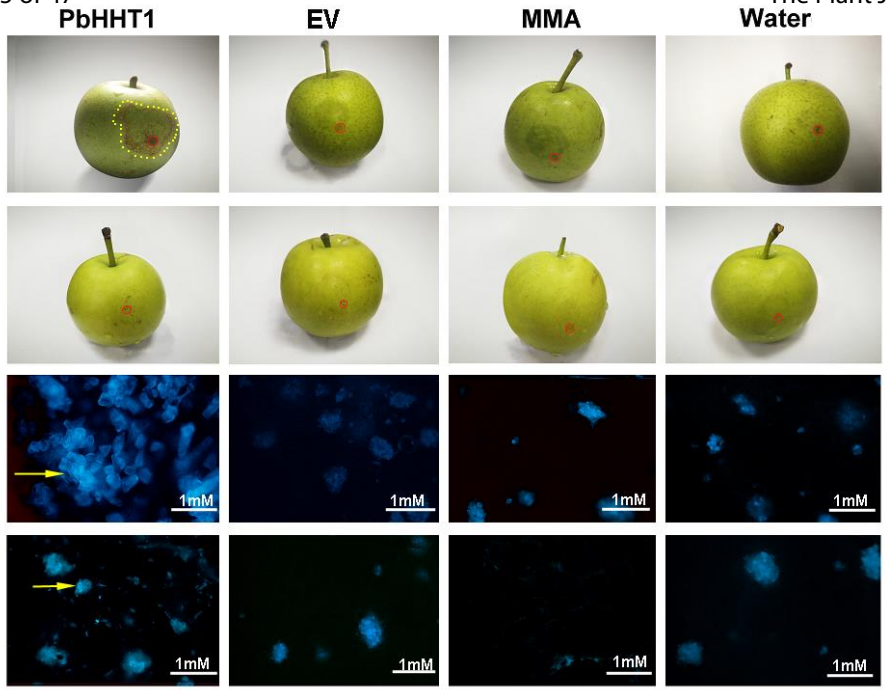

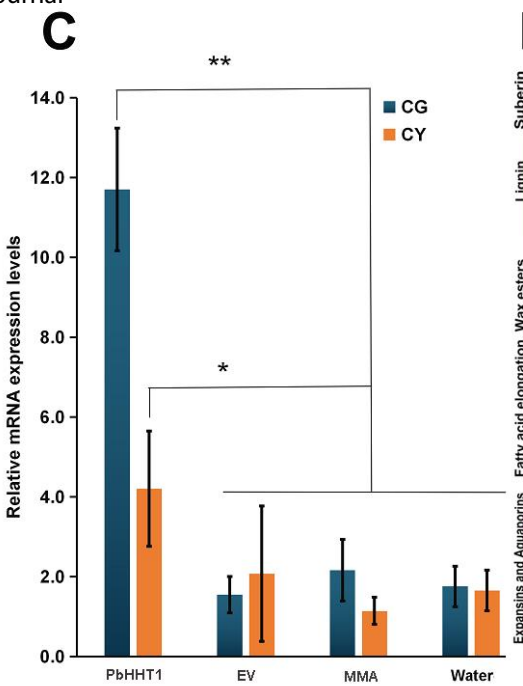

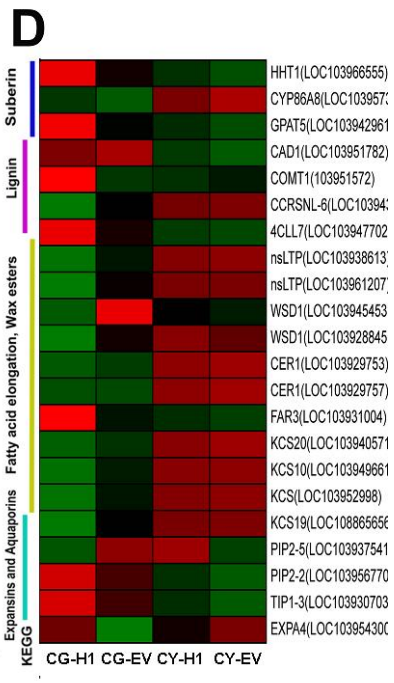

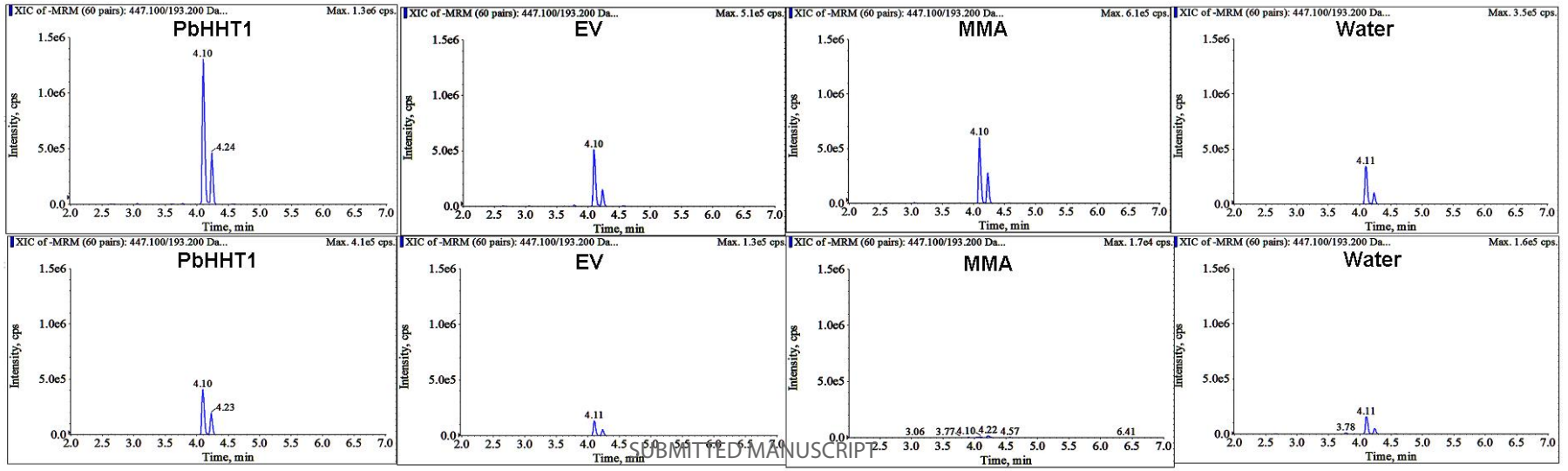

SUBMITTED MANUSCRIPT

Fig 7

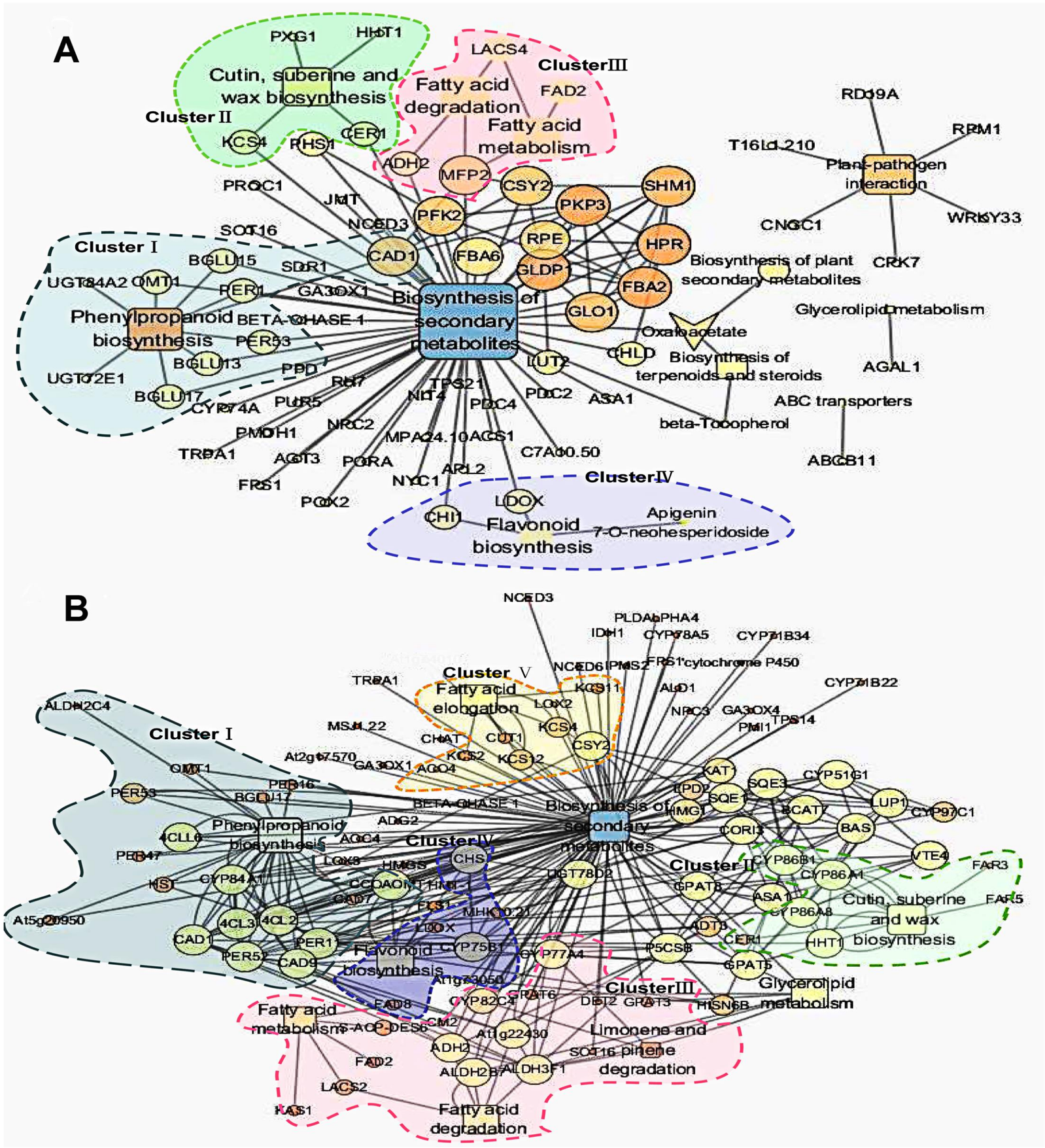
A
Cutin, suberine and wax biosynthesis
Cluster II
Fatty acid degradation
Fatty acid metabolism
ClusterIII
Cluster I
Phenylpropanoid biosynthesis
Biosynthesis of secondary metabolites
Flavonoid biosynthesis
ClusterIV
Plant-pathogen interaction
Biosynthesis of plant secondary metabolites
Glycerolipid metabolism
Oxaloacetate
Biosynthesis of terpenoids and steroids
ABC transporters
beta-Tocopherol
PXG1
HHT1
LACS4
FAD2
KCS4
CER1
RHS1
ADH2
MFP2
CSY2
SHM1
PKP3
PFK2
PROC1
JMT
NCED3
SOT16
CAD1
FBA6
RPE
HPR
GLDP1
FBA2
GLO1
BGLU15
SDR1
UGT84A2
OMT1
PER1
GA3OX1
BETA-GHASE 1
PER53
BGLU13
UGT72E1
BGLU17
PPD1
RD7
TPS21
NIT4
PDC4
PDC2
ASA1
CHLD
LUT2
CYP74A
PUR5
PMDH1
NRC2
MPA24.10
ACS1
C7A00.50
TRFA1
AGT3
PGRA
ARL2
FRS1
NYC1
PGX2
LDOX
CHI1
Apigenin
7-O-neohesperidoside
RD19A
RPM1
T16L1.210
CNGC1
WRKY33
CRK7
AGAL1
ABCB11
B
NCED3
PLDALPHA4
IDH1
CYP78A5
CYP71B34
FRS1
cytochrome P450
CYP71B22
NCED6
PMS2
KCS11
ALD1
NRC3
GA3OX4
PMI1
TPS14
TRFA1
Cluster V
Fatty acid elongation
LOX2
KCS4
CHAT
CUT1
CSY2
KCS2
KCS12
MSH1.22
At2g47570
GA3OX1
AGO4
ALDH2C4
Cluster I
OMT1
PER53
PER16
BGLU17
BETA-GHASE 1
Phenylpropanoid biosynthesis
ADG2
4CLL6
AGC4
PER47
LOX6
HMGS
CHS
HST
CYP84A1
CCOAOMT1
HCT1
CAD7
FLS1
MHK10.21
At5g20950
4CL3
4CL2
LDOX
CAD1
PER1
PER52
CAD9
Flavonoid biosynthesis
CYP75B1
CYP77A4
At1g63050
GPAT6
ClusterIII
CYP82C4
DGT2
GPAT3
HISN6B
Glycerolipid metabolism
Fatty acid metabolism
FAD8
ECR
KAR
HACD
DES6
CM2
At1g22430
ADH2
FAD2
ALDH2B7
ALDH3F1
Limonene and pinene degradation
SOT16
LACS2
KAS1
Fatty acid degradation
KAT1
IPDP
SQE3
CYP51G1
SQE1
IMGT
LUP1
CYP97C1
BCAT7
CORI3
BAS
VTE4
ClusterII
CYP86B1
FAR3
DGT78D2
CYP86A1
GPAT8
ASA1
FAR5
CYP86A8
Cutin, suberine and wax biosynthesis
ADT5
CER1
HHT1
P5CS8
GPAT5

Fig 8

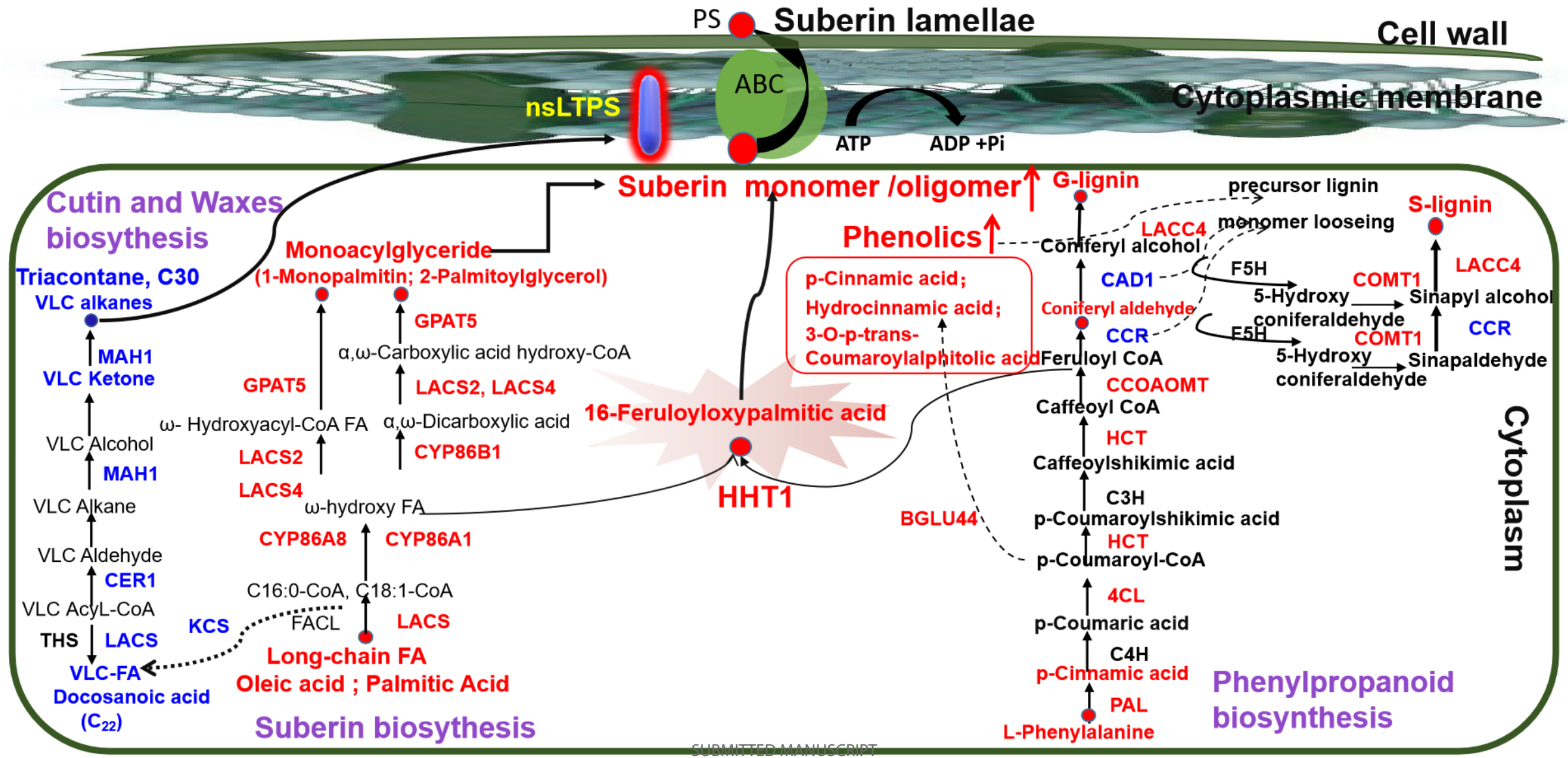
PS
Suberin lamellae
Cell wall
Cytoplasmic membrane
nsLTPS
ABC
ATP
ADP +Pi
Suberin monomer /oligomer
Cutin and Waxes biosynthesis
Triacontane, C30
VLC alkanes
MAH1
VLC Ketone
VLC Alcohol
MAH1
VLC Alkane
VLC Aldehyde
CER1
VLC AcyL-CoA
THS
LACS
VLC-FA
Docosanoic acid
(C22)
Monoacylglyceride
(1-Monopalmitin; 2-Palmitoylglycerol)
GPAT5
α,ω-Carboxylic acid hydroxy-CoA
LACS2, LACS4
ω- Hydroxyacyl-CoA FA
α,ω-Dicarboxylic acid
CYP86B1
LACS2
LACS4
ω-hydroxy FA
CYP86A8
CYP86A1
C16:0-CoA, C18:1-CoA
FACL
LACS
KCS
Long-chain FA
Oleic acid ; Palmitic Acid
Suberin biosythesis
16-Feruloyloxypalmitic acid
HHT1
Phenolics
p-Cinnamic acid;
Hydrocinnamic acid;
3-O-p-trans-
Coumaroylalphitolic acid
BGLU44
G-lignin
Coniferyl alcohol
CAD1
Coniferyl aldehyde
CCR
Feruloyl CoA
CCOAOMT
Caffeoyl CoA
HCT
Caffeoylshikimic acid
C3H
p-Coumaroylshikimic acid
HCT
p-Coumaroyl-CoA
4CL
p-Coumaric acid
C4H
p-Cinnamic acid
PAL
L-Phenylalanine
LACC4
precursor lignin
monomer looseing
F5H
5-Hydroxy coniferaldehyde
COMT1
Sinapyl alcohol
CCR
Sinapaldehyde
S-lignin
LACC4
F5H
5-Hydroxy coniferaldehyde
COMT1
Cytoplasm
Phenylpropanoid biosynthesis